

## TOPICAL REVIEW

# Mechanisms of cluster ionization in strong laser pulses

U Saalmann<sup>1</sup>, Ch Siedschlag<sup>2</sup> and J M Rost<sup>1</sup><sup>1</sup> Max Planck Institute for the Physics of Complex Systems, Nöthnitzer Straße 38,  
01187 Dresden, Germany<sup>2</sup> FOM Institute for Atomic and Molecular Physics, Kruislaan 407, 1098 SJ Amsterdam,  
The NetherlandsE-mail: [us@pks.mpg.de](mailto:us@pks.mpg.de)

Received 20 October 2005, in final form 22 November 2005

Published 18 January 2006

Online at [stacks.iop.org/JPhysB/39/R39](http://stacks.iop.org/JPhysB/39/R39)**Abstract**

Femtosecond laser pulses have proven to provide valuable insight into the dynamics of microscopic systems by using pump–probe techniques. Applied to atomic clusters even a single pulse of varying pulse duration can reveal how and when energy from the laser pulse is transferred effectively to the cluster. We review the main experimental observables for energy transfer to a cluster and the major theoretical approaches which have been devised. Most importantly, we compare the cluster response to standard 780 nm light pulses with the response to 100 nm pulses, already obtained at a VUV free electron laser (FEL) source, and with 3 nm light which will be available from x-ray FEL sources.

(Some figures in this article are in colour only in the electronic version)

**Contents**

1. Introduction	40
2. Experimental techniques for probing ionization mechanisms	42
2.1. Experimental observables	42
2.2. Experiments in the IR domain	42
2.3. Experiments in the VUV domain	46
3. Theoretical approaches for laser–cluster interaction	48
3.1. Hamilton operator	48
3.2. Perturbative and non-perturbative laser–atom interaction	48
3.3. Quantum-mechanical description using DFT	50
3.4. Nano-plasma model	52
3.5. Quasi-classical microscopic description	54

4. Infrared regime (780 nm)	57
4.1. Cooperative behaviour in small clusters	57
4.2. Collective behaviour in medium-sized clusters	59
4.3. Nonlinear behaviour in large clusters	61
5. VUV regime (100 nm)	63
5.1. Quasi-classical models	64
5.2. Thomas–Fermi calculations	67
5.3. Statistical modelling	68
6. X-ray regime (3 nm)	68
6.1. Clusters versus atoms	69
6.2. Secondary ionization effects in clusters	70
6.3. Explosion dynamics	73
7. Summary	74
References	75

## 1. Introduction

The interaction of clusters with intense laser pulses has led to some very interesting observations, from the production of highly charged ions, energetic electrons and ions, over x-rays to neutrons. The latter particles are a consequence of probably the most spectacular effect, namely deuterium fusion in a mixture of argon–deuterium clusters as a consequence of irradiation with light. These phenomena indicate a very efficient energy transfer of light to the charged particles (electrons and ions) in the cluster which is rooted in its nature; between the condensed and the gas phase, a cluster is much denser than a gas, thus absorbing more energy than isolated particles. Yet, it does not have as many dissipation channels, e.g., lattice vibrations, as a solid.

The strange nature of a cluster renders its research quite naturally an interdisciplinary endeavour where important contributions come from different fields. The scientists who are involved have a physics background which reaches from chemistry over nuclear physics, atomic physics, quantum optics, plasma physics to condensed matter physics. Consequently, the concepts applied and the nomenclature used differ considerably. This leads sometimes to difficulties since it may be not clear if two concepts are more or less identical and just distinguished by a different language or if they are truly different. Another complication arises from the wealth of variables which can be changed, even in the experiment, when shining laser pulses on clusters.

Hence, a restriction of topics is necessary when trying to summarize the field. The title of the review already indicates our main goal. This goal we will pursue mainly for rare-gas clusters which contain a couple of atoms up to large clusters whose size is limited only by the condition that propagation effects of the incident light do not play a role. In other words, we take full transparency of the cluster with respect to the light for given and will not address phenomena such as skin depth, etc, which are characteristic for extended plasmas. Furthermore, we will concentrate on a few important observables, such as charge states of ions and kinetic energy of ions and electrons to highlight the major phenomena of energy transfer in cluster–laser interaction. Here, we will put an emphasis on such phenomena which are sensitive to the pulse length, and in turn, permit a deeper insight into the time-dependent evolution of the cluster dynamics. To this end, we will discuss a selection of published experiments and theoretical papers.

What we will also address in some detail is the dependence of energy transfer the cluster on the wavelength of the light. The physics changes dramatically when going from the canonical

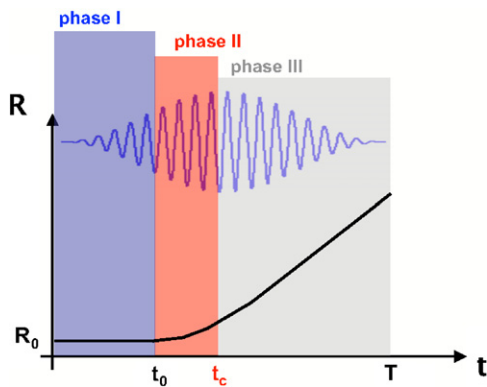


**Figure 1.** Sketch of cluster dynamics under a strong laser pulse in terms of the time-dependent cluster radius  $R(t)$ . Atomic ionization (phase I), critical expansion (II) and relaxation (III); see text. The laser pulse is also indicated.

780 nm, given by Ti:sapphire light, over 100 nm, which was the first wavelength provided by the free electron laser (FEL) in Hamburg, to intense light of 3 nm which will be available in the future. Naturally, most published work which we will review deals with 780 nm, a handful of papers address the 100 nm situation and only little research has been conducted so far in the range of 3 nm light.

This focus distinguishes the present topical review from existing reviews which deal with cluster dynamics induced by excitation of core levels in the cluster atoms (Rühl 2003) or with the exposure of rare-gas atom clusters to very strong laser pulses whose peak field strength exceeds the atomic unit at a wavelength of 780 nm (Krainov and Smirnov 2002). In the latter, general techniques and concepts are reviewed which are also relevant for what we discuss here. Ultrafast cluster dynamics with short but not very intense pulses has been discussed from a chemical perspective by Dermota *et al* (2004).

Common to all clusters subjected to laser pulses of different wavelengths, provided they are strong enough, is the three-step scenario sketched in figure 1. In the first phase (termed I), the light couples to the atoms as if they were isolated, the cluster environment does not have an effect. In phase II, the critical and interesting phase, the cluster expands due to the ions created in phase I leading to a decreasing density of ions. On the other hand, the density of so-called ‘quasi-free’ electrons in the cluster does not necessarily decrease. These electrons are said to be ‘inner ionized’ but not yet ‘outer ionized’, i.e., they are still bound to the cluster but no longer to a specific ion. The net change of their density depends on the balance of inner and outer ionization at each instant of time. Finally, in phase III the absorption of energy from the laser pulse has come to an end, as the pulse becomes very weak and finally goes to zero. During phase III, energy is redistributed within the cluster, e.g., through recombination. The cluster completely disintegrates and the final (measurable) distribution of ions and electrons is built up. This relatively simple yet quite universal scheme facilitates the understanding and assessment of the very different mechanisms of energy absorption we will discuss.

In the next section, we discuss the key experiments and their findings, first for 780 nm light and then for VUV light. In section 3, we explain the main theoretical concepts which have been used over the last years. They reach from quantum approaches with density functional methods over mixed quantum–classical to full classical approaches, where the latter two can be grouped according to microscopic and macroscopic descriptions. Equipped with the experimental and theoretical foundations, sections 4–6 deal explicitly with clusters in infrared

(780 nm), VUV (100 nm) and x-ray light (3 nm). The review ends with a summary and outlook in section 7.

## 2. Experimental techniques for probing ionization mechanisms

### 2.1. Experimental observables

The laser fields considered here are so strong that they ultimately lead to a complete breakup of the cluster into single ions and electrons. In principle, accessible experimentally are the final charge and vectorial velocity distributions of the fragments, or from the latter, the energy as well as the angular distributions. Out of this multitude of information, meaningful quantities have to be extracted which can provide insight into the explosion dynamics and the way how energy is transferred to the cluster. These have mostly been the average/highest charge states of the exploding ions (Snyder *et al* 1996, Lezius *et al* 1998, Köller *et al* 1999, Wabnitz *et al* 2002, Zamith *et al* 2004) or the kinetic energies of the ions and electrons (Shao *et al* 1996, Springate *et al* 2000, Kumarappan *et al* 2001, Chen *et al* 2002, Fukuda *et al* 2003, Hirokane *et al* 2004). Neutrons, which result from the fusion of fast fragments of deuterium clusters, have been measured (Ditmire *et al* 1999, Zweiback *et al* 2000, Grillon *et al* 2002, Madison *et al* 2004).

Instead of using particle properties, one can measure the energy transferred to the cluster by recording how much laser light has been absorbed by the clustered medium (Ditmire *et al* 1997, Chen *et al* 2002). The latter approach has the advantage that the kinetic energy of neutral atoms, which are usually not detected, is implicitly included. Yet another indicator of the efficient energy transfer to the cluster is its emission of photons due to recombination of highly charged ions. Measurements have shown photons from XUV up to x-ray energies (McPherson *et al* 1994, Schroeder *et al* 1998, Parra *et al* 2000, Mocek *et al* 2000, Ter-Avetisyan *et al* 2001, Junkel-Vives *et al* 2002, Lamour *et al* 2005, Dorchies *et al* 2005).

Comparison between theory and experiment suffers from a two-fold difficulty: first, most cluster beams never consist of clusters with a single size. Rather, only the mean of a distribution of cluster sizes can be controlled by changing the backing pressure; the mean size can be obtained from the so-called Hagena parameter (Hagena and Obert 1972) and the distribution in the beam can be characterized by Rayleigh scattering (Ditmire *et al* 1998). Second, femtosecond laser pulses have a spatial intensity profile, so that not all clusters experience the same electric field. One might argue that the latter complication can be removed when choosing the highest ionic charge states as the final observable, since it seems reasonable to assume that these charge states are produced only in the laser focus. However, this is not necessarily true; later we will encounter situations, where, depending on the expansion dynamics of a cluster, pulses with smaller peak intensities can lead to higher charge states than pulses with higher peak intensities.

### 2.2. Experiments in the IR domain

In the following, we want to summarize briefly some of the experiments which have dealt with the question of the interaction of clusters with femtosecond IR lasers. The collection is by no means complete, and we apologize to those whose work could not be included here.

Early experiments demonstrated that, in general, clusters do not survive the irradiation by IR light with an intensity higher than about  $10^{12}$ – $10^{13}$  W cm<sup>-2</sup>. Instead, they undergo complete fragmentation/Coulomb explosion emitting surprisingly many highly charged ions and energetic particles, along with x-ray radiation (Ditmire *et al* 1996). These findings focused

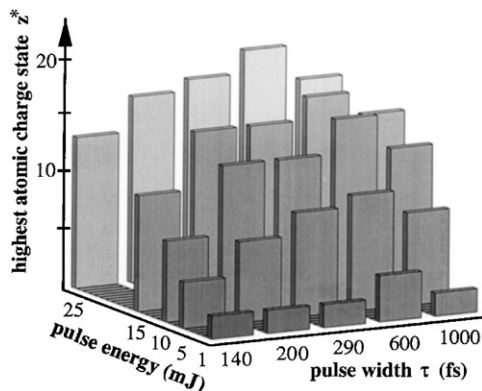


**Figure 2.** Highest charge states observed for irradiated platinum clusters as a function of pulse width and energy (from Köller *et al* (1999)).

the subsequent research efforts on the question of efficient energy absorption mechanisms in clusters (Ditmire 1998, Lezius *et al* 1998). Most recent experiments have provided a time-resolved mapping of the explosion process by varying the length of the femtosecond laser pulse (Köller *et al* 1999, Parra *et al* 2000, Kumarappan *et al* 2002, 2003a, Lamour *et al* 2005) or by using a pump–probe setup. In the latter, a first short laser pulse triggers the expansion followed after variable delay by a second pulse. Thereby, the absorption efficiency of the expanding cluster can be probed (Zweiback *et al* 1999, Springate *et al* 2000, Kim *et al* 2003, Döppner *et al* 2005) since the explosion of the cluster ions and hence the change of the cluster radius takes place on a femtosecond time scale.

**2.2.1. Pulse length dependence.** One example of an experiment in which the pulse length has been varied has been performed by Meiwes-Broer and co-workers (Köller *et al* 1999). Platinum clusters with an average size of  $N \approx 20$  and a size distribution which did not extend beyond  $N = 100$  were irradiated by a femtosecond Ti:sapphire laser. While the pulse energy (ranging from 1 mJ to 25 mJ) was kept fixed, the pulse length could be varied from 140 fs to several ps. The intensity in the focus could be as high as  $10^{16} \text{ W cm}^{-2}$ . The time-of-flight spectrum showed, besides small singly and doubly charged cluster fragments originating from spatial areas with lower laser intensity, platinum ions with charges of up to  $q = 20$ , while only  $q = 4$  was observed when ionizing single platinum atoms. The main outcome of this experiment was, however, that a pulse length of  $T \approx 600$  fs produced the highest charge states, although, due to the boundary condition of constant pulse energy, the field intensity at this pulse length was about a factor of 7 smaller than for the shortest pulses. The observed maximum charge states as a function of pulse width and pulse energy are shown in figure 2. Since platinum, i.e. metal clusters were used, these findings were interpreted in terms of a plasmon frequency which decreases in time due to the cluster expansion. Eventually, plasmon and laser frequencies coincide, leading to resonant absorption.

Zweiback *et al* (1999) used xenon and argon clusters of about  $10^5$  atoms per cluster and exposed them to pulses of variable length with constant pulse energy as well as to pump–probe type pulses. Due to the much bigger size of the clusters compared to the platinum experiment, field intensities of several  $10^{17} \text{ W cm}^{-2}$  could be applied without reaching saturation. The measured observable was the absorption of laser energy by the clustered medium. As in the platinum cluster experiment, an optimal pulse length (or an optimal pump–probe delay,

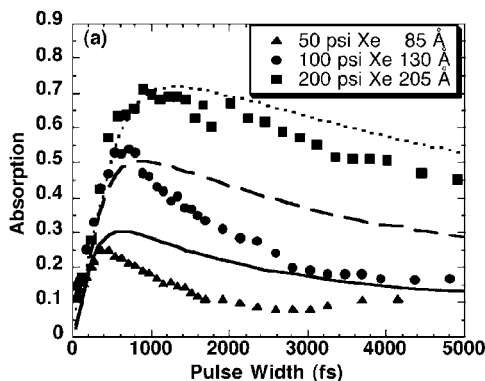


**Figure 3.** Absorption as a function of pulse length for different gas pressures, i.e. different cluster sizes (from Zweiback *et al* (1999)). The average cluster radii are 85, 130 and 205 Å, respectively. Solid lines are the results of calculations based on a nano-plasma model; see section 3.4.

respectively)  $T_{\text{crit}}$  was found, cf figure 3, and related to the existence of a critical cluster radius  $R_{\text{crit}}$ . Absorption was seen to increase by more than 50% when going from very short pulses/delays to  $T_{\text{crit}}$ , reaching up to 70% under optimal conditions. The results were explained by assuming that such big clusters quickly turn into nano-plasma balls during the leading edge of the pulse. Hence, the electron cloud can be resonantly excited when the surface plasma frequency matches the laser frequency. More details concerning the theoretical explanation, and also the relation between the surface plasma and the plasmon picture, will be given in section 4.2. Important contributions with a single pulse of variable length have also been made by Mathur and his group (Kumarappan *et al* 2002, 2003a). These results will be discussed in more detail when we come to differential measurements.

First measurements of soft x-ray emission from small neon clusters undergoing intense IR irradiation with a pulse length varied from 25 to 100 fs (Mocek *et al* 2000) showed that the x-ray yield increased when increasing the pulse length. Unfortunately, the prediction that this increase can again be traced back to an optimal cluster radius could not be verified in this case because the pulse length could not be increased beyond 100 fs, which made an eventual decrease in the yield for longer pulse lengths unobservable. Recent experiments concerning x-ray generation (Lamour *et al* 2005) could cover a larger range of pulse lengths showing a clear maximum of the absolute yield of keV photons at about 130 fs for argon clusters and 200–300 fs for xenon clusters, which, remarkably, was found to be relatively insensitive to the cluster size.

**2.2.2. Pump–probe type experiments.** Using two pulses instead of only one has the advantage that possible multiple occurrences of increased absorption during the expansion of the cluster can be resolved. Furthermore, the instant of time at which (locally) optimal energy coupling conditions are realized can be determined more precisely with two relatively narrow pulses than with one broad pulse of varying length. Such a pump–probe type scenario has been used in the experiment already described (Zweiback *et al* 1999). A similar pump–probe setup was used to study the explosion of acetone monomers and clusters (Snyder *et al* 1996). There, beating patterns were found when measuring the number of charged  $\text{O}^{q+}$  ions as a function of probe delay. These minima and maxima were attributed to the ionization being very sensitive to the internuclear distance, thus ruling out the nano-plasma model (or coherent electron motion model as it was termed by Snyder *et al* (1996)) under the conditions of that experiment and

giving a first hint towards the connection of enhanced ionization with cluster explosion. The Rostock group (Döppner *et al* 2000) extended its studies to the dynamics of lead and platinum clusters in a pump–probe situation, and most recently, to silver clusters (Döppner *et al* 2005). When using platinum clusters with an average size of  $N \approx 50$ –100 atoms and a peak intensity of  $10^{15} \text{ W cm}^{-2}$ , an optimal delay time of about 1 ps was observed. This result as well as the more recent results on silver clusters (Döppner *et al* 2005) was interpreted as a further confirmation of the plasmon resonance being hit by the probe pulse.

Finally, Zamith *et al* (2004) performed an optimal control experiment which *a posteriori* also has to be classified as being of pump–probe type. Using a pulse shaper with 80 parameters, the production of charge states  $q > 11$  from large clusters,  $\langle N \rangle = 1.6 \times 10^4$ , was optimized using a genetic algorithm. Interestingly, the laser pulse, which could be as intense as  $5 \times 10^{15} \text{ W cm}^{-2}$  in the Fourier transform limited case, splits up into *two* 120 fs peaks with a delay of about 500 fs, i.e. the optimal pulse shape for the production of highly charged ions turned out to be of pump–probe type. Naturally, these findings were again explained by the surface plasma resonance.

**2.2.3. Differential measurements.** The experiments described so far have mostly concentrated on rather global observables such as the laser absorption or the highest ionic charge state. Also, the fact that for a certain pulse length or pump–probe delay, respectively, these observables show a maximum may hint towards a critical internuclear distance, but gives *a priori* no information about the mechanism which causes this internuclear distance. Hence, it is necessary to look at more differential quantities in order to better understand the explosion process.

Lezius *et al* (1998) measured the time of flight (or, equivalently, the kinetic energy) of the ions resulting from the irradiation of large argon and xenon clusters with a single IR pulse of  $I = 10^{17} \text{ W cm}^{-2}$  as a function of  $q$ , the ionic charge. The question they investigated was whether the kinetic energy of the ions is produced mainly by Coulomb explosion (in which case one would expect  $E_{\text{kin}} \sim q^2$  due to the inter-ionic Coulomb potential) or by hydrodynamic expansion, which means that the ions are accelerated by the electron cloud, so that one would expect  $E_{\text{kin}} \sim q$ . The first mechanism should dominate in small clusters (and molecules); the latter one would be responsible for the expansion of large clusters. The experimental observation was mixed; whereas for argon clusters a clear  $q^2$  dependence of the kinetic energy was observed, in the xenon case the highest charged ions exhibited an  $E_{\text{kin}}$  which was linearly proportional to  $q$ , hence suggesting that these highest charges are mainly accelerated hydrodynamically. Kumarappan *et al* (2003b) performed a similar experiment using water, argon and xenon clusters. While the water clusters were rather small  $N \approx 60$ , the rare-gas clusters contained  $N > 10^4$  atoms. According to conventional wisdom, it was expected that the kinetic energy of the  $\text{O}^{q+}$  ions resulting from the disintegration of the water clusters should be proportional to  $q^2$ . In contrast, the ions from big rare-gas clusters, which could support an ‘electron fluid’, should be accelerated hydrodynamically. However, it turned out that in *all* cases the kinetic energy of the ions increased linearly with  $q$ ; this result leads to a reanalysis of the explosion mechanism by Kumarappan *et al* (2003b), and they correctly stated that it is only the *average* kinetic energy of the ions which should scale with  $q^2$  in the case of a pure Coulomb explosion. The individual kinetic energy of a specific ion will, on the other hand, always scale linearly with its charge, so that the conclusion had to be that the dependence of  $E_{\text{kin}}$  on  $q$  was not an appropriate observable to distinguish between hydrodynamic and Coulomb-driven expansion. The same authors have also collected experimental evidence which showed that the simple spherically symmetric nano-plasma model for large clusters is not sufficient to explain the angular distribution of the exploding ions (Kumarappan *et al*

2002, 2003a). While ions with low kinetic energy were ejected isotropically, it was discovered that the ions with the highest kinetic energy, carrying also the largest positive charge, are preferably emitted along the laser polarization axis. Treating the electrons and ions of the cluster as two oppositely charged spheres, one sees that ions whose origin is the surface of the cluster experience a higher net force than other ions along the polarization axis. This explains why ions emitted along this direction acquire the highest kinetic energies.

One of the main predictions of the nano-plasma model (Ditmire *et al* 1996), cf section 3.4 for details, was the appearance of hot electrons resulting from the instant of time when the resonance condition is fulfilled. This prediction seemed to be verified when the energy distribution of the ionized electrons resulting from the interaction of large Xe clusters with an intense femtosecond IR laser was recorded (Shao *et al* 1996); beside a broad peak of electrons with energies of a few hundred eV, a spike at  $\approx 2$  keV was observed, which was taken to be a clear signature for a nano-plasma resonance. Later measurements (Springate *et al* 2003, Kumarappan *et al* 2003a) could, however, not reproduce this result; the fact that the second peak appeared in the time-of-flight signal at the same position with the same strength when varying parameters such as gas expansion conditions, laser pulse duration and focusing made Springate *et al* (2003) believe that it is not electrons which cause this feature, but rather photons with energies in the UV or XUV range.

To summarize this section, the common features of virtually all experiments in femtosecond IR–cluster interaction are (a) the fact that clusters absorb laser energy orders of magnitude better than single atoms with the consequence that the cluster usually disintegrates completely into fast electrons and highly charged ions, since—in contrast to bulk material—the absorbed energy cannot dissipate, and (b) the observation of a critical time  $T_{\text{crit}}$  at which the efficiency of energy coupling is enhanced. The attempts to find clear experimental evidence to distinguish between the two main theoretical models for the occurrence of  $T_{\text{crit}}$ , i.e. enhanced ionization and collective resonance, have, however, not really succeeded so far. Broad cluster size distributions and the spatial laser intensity profile render direct comparisons between experiment and theory rather difficult. Nevertheless, a relatively clear picture has emerged on the theoretical side as to which mechanism applies in which parameter regime. This will be the topic of section 4.

### 2.3. Experiments in the VUV domain

Until very recently, experiments with short, intense laser pulses were only possible in the IR or UV domain. With the advent of the free electron laser (FEL) which uses self-amplified spontaneous emission (Treusch and Feldhaus 2003), it has become possible to generate comparably intense laser fields also in the VUV domain. Using the first stage of the x-ray free electron laser at DESY, Möller and co-workers (Wabnitz *et al* 2002) performed the first experiment on the interaction of intense soft x-ray pulses with rare-gas clusters. The FEL delivered photons with 12.7 eV at an intensity up to  $7 \times 10^{13}$  W cm<sup>-2</sup>; the pulses were 100 fs long. Single xenon atoms and xenon clusters with size from  $N \approx 80$  to  $N \approx 30\,000$  were irradiated with the FEL radiation, and the resulting electrons and ions were detected in a time-of-flight spectrometer. Xenon was chosen because the photon energy is big enough to singly ionize a xenon atom with one photon (the first ionization energy of xenon is 12.2 eV). The measured time-of-flight spectra for single xenon atoms and a variety of xenon cluster sizes are shown in figure 4. The first important observation is that no clustered fragments are detected, i.e., the clusters disintegrate completely into charged ions and electrons. Secondly, the charge of the xenon

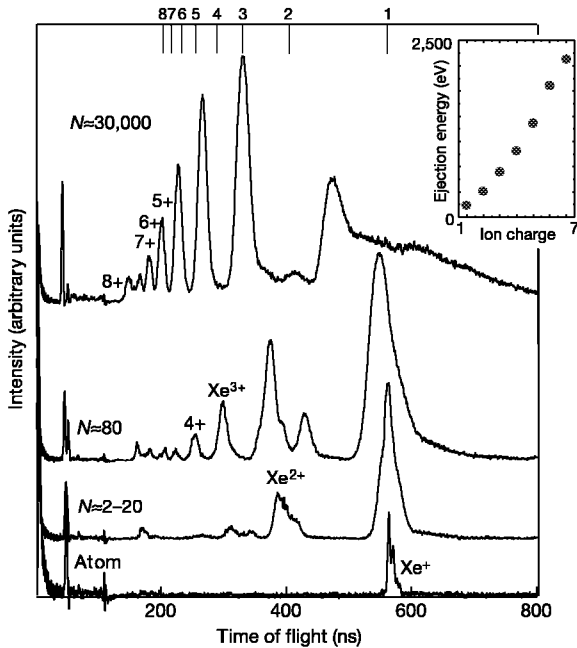


**Figure 4.** Time-of-flight spectra of the ionization products for single xenon atoms and xenon clusters of different sizes (from Wabnitz *et al* (2002)).

ions can be as high as 8+ for clusters of  $N \approx 30\,000$  reaching still at least 4+ for smaller clusters of  $N \approx 80$ . The ions acquire kinetic energies of several keV, as the inset in figure 4 shows. Irradiating single xenon atoms leads, however, only to singly charged ions<sup>3</sup>.

These results are rather surprising if one tries to understand the experiment in terms of the modelling that has been developed for the IR case: tunnelling and therefore enhanced ionization cannot play a role in the ionization process since the Keldysh parameter  $\gamma > 1$ ; cf table 2 and section 3.2. Efficient energy coupling via a plasmon resonance can also be ruled out. Taking  $\Omega = \sqrt{Nq/R^3}$  as an approximation for the surface plasma frequency, cf equation (30) and its discussion, of a cluster with radius  $R$  consisting of  $N$  ions with charge  $q$  each (so that the total number of electrons is  $Q = Nq$ ), it turns out that one would have to assume an average ionic charge of  $q = 16$  for a xenon cluster in its neutral configuration to yield a surface plasma frequency of 12.7 eV. Nevertheless, an approximate calculation of the energy absorbed by a  $\text{Xe}_{1500}$  cluster yielded an average of 400 eV per atom, an order of magnitude higher than what came out of a simple quasi-classical simulation done by Wabnitz *et al* (2002).

The same experiment has also been carried out for argon clusters (Laarmann *et al* 2004). Two things could be learned from this work. Although the first ionization threshold of argon is larger than the energy of a single VUV photon (namely 15.75 eV), there was no qualitative difference between xenon and argon clusters once the FEL intensity was bigger than

<sup>3</sup> It should be mentioned that the experiment has been repeated with a slightly altered setup which showed xenon ions up to  $q = 6$  resulting from single atoms (Wabnitz *et al* 2005). The cluster results remained unchanged. It has been suspected that the mode structure of the FEL has changed between the two experiments. This would be a possible explanation for the increased multiphoton absorption in the single atom case (Wabnitz 2004). Furthermore, the spectra shown in the first paper (Wabnitz *et al* 2002) have not been corrected for the different sensitivities of the TOF detector to the ionic charge states.

$10^{12} \text{ W cm}^{-2}$ . Secondly, for sufficiently high intensity the time-of-flight signal does not change when slightly varying the FEL photon frequency. Especially, when the photon frequency was tuned to the surface (105 nm) or the bulk (100.8 nm) excitation, the ion yield was practically identical to the off-resonant case. Only for a low intensity of  $I \approx 10^{11} \text{ W cm}^{-2}$  does the effect of the electronic structure of the cluster became important. The minor role of the electron structure certainly encourages a quasi-classical description of intense field–cluster interaction also in the VUV regime; some theoretical approaches in this direction will be discussed in section 5.

### 3. Theoretical approaches for laser–cluster interaction

The purpose of this section is twofold. (i) We discuss the description of intense laser–*atom* interaction with emphasis on the different mechanisms of ionization when going from infrared via VUV to x-ray laser wavelengths. Understanding this interaction is also directly relevant to describe clusters since the strongly localized electrons in rare-gas clusters as well as the core electrons in metal clusters behave like atomic electrons. (ii) We summarize approaches that have been used in the last years to tackle the response of many-atom systems like *clusters* to strong laser impact.

#### 3.1. Hamilton operator

The Hamiltonian of an atomic cluster exposed to a strong laser field reads (we use atomic units)

$$\hat{H} = \sum_K \frac{1}{2M} \mathbf{P}_K^2 + \sum_{K>L} W(\mathbf{R}_K - \mathbf{R}_L) + \sum_k \frac{1}{2} (\mathbf{p}_k - \mathcal{A}(t))^2 + \sum_{K>k} V(\mathbf{R}_K - \mathbf{r}_k) + \sum_{k>l} w(\mathbf{r}_k - \mathbf{r}_l), \quad (1)$$

where  $M$  is the nuclear mass. Whether momenta and positions of the nuclei  $\{\mathbf{P}_K, \mathbf{R}_K\}$  and the electrons  $\{\mathbf{p}_k, \mathbf{r}_k\}$  are treated quantum mechanically or classically remains open in equation (1). Usually, nuclei are treated classically while for the electrons quantum as well as classical descriptions<sup>4</sup> have been used. Nuclei and electrons interact among themselves through  $W$  and  $w$ , respectively, and among each other through  $V$ . The laser couples to the electrons, its coupling to the nuclei is negligible due to their large mass. The coupling is formulated in a ‘semi-classical’ way, in the minimal coupling scheme, i.e., the laser is treated as a classical field given by the vector potential  $\mathcal{A}$  which modifies the electron momenta (Mittleman 1993). Furthermore, we adopt the dipole approximation right from the beginning. For optical wavelengths this is always justified, even for larger clusters. For x-ray wavelength this applies as well since the interaction is predominantly with inner-shell electrons with a spatial extension smaller than the wavelength. Interaction of x-ray fields with delocalized electrons is negligible, see the discussion at the end of section 3.5.3.

#### 3.2. Perturbative and non-perturbative laser–atom interaction

For the following discussion, it is sufficient to consider an atom with just one electron moving in an effective potential  $V_1$  which accounts for the attraction of the nucleus and the interaction with all the other electrons; one could also think of an atom embedded in a plasma environment (Micheau *et al* 2005). The Hamiltonian for this so-called single-active-electron approximation (Kulander 1988, Lambropoulos *et al* 1998) reads

$$\hat{H}_1 = \frac{1}{2} (\hat{\mathbf{p}} - \mathcal{A}(\mathbf{r}, t))^2 + V_1(\mathbf{r}). \quad (2)$$

<sup>4</sup> Electrons can be treated classically when their energy is larger than the Fermi energy.

Instead of solving the Schrödinger equation  $i\frac{\partial}{\partial t}\psi(\mathbf{r}, t) = \hat{H}_1\psi(\mathbf{r}, t)$  with the Hamilton (2), it is advantageous to make a unitary transformation (Mittleman 1993)

$$\psi(\mathbf{r}, t) \rightarrow \psi'(\mathbf{r}, t) = \exp(-i\mathcal{A}(t) \cdot \mathbf{r})\psi(\mathbf{r}, t) \quad (3)$$

to get a ‘new’ Schrödinger equation  $i\frac{\partial}{\partial t}\psi'(\mathbf{r}, t) = \hat{H}'_1\psi'(\mathbf{r}, t)$  with

$$\hat{H}'_1 = \frac{1}{2}\hat{\mathbf{p}}^2 + V_1(\mathbf{r}) + \frac{\partial\mathcal{A}(t)}{\partial t} \cdot \mathbf{r} = \frac{1}{2}\hat{\mathbf{p}}^2 + V_1(\mathbf{r}) - \mathcal{E}(t) \cdot \mathbf{r} \equiv \hat{H}_0 - \mathcal{E}(t) \cdot \mathbf{r}. \quad (4)$$

We will consider the laser interaction term as a perturbation to the atomic Hamiltonian  $\hat{H}_0$  and ask under which conditions the perturbative picture holds. One can write the amplitude for the transition from one eigenstate  $\phi_i$  to another eigenstate  $\phi_f$  of  $\hat{H}_0$  as a perturbation series. For a monochromatic field  $\mathcal{E}(t) = \mathcal{E} \cos(\omega t)$  an  $n$ th-order term of this series looks like (Faisal 1987)

$$T_{fi}^{(n)} = \mathcal{E}^n \langle \phi_f | DG(\varepsilon_{n-1}) DG(\varepsilon_{n-2}) D \cdots DG(\varepsilon_1) D | \phi_i \rangle, \quad (5)$$

with the dipole operator  $D = \mathbf{r} \cdot \boldsymbol{\mathcal{E}}/\mathcal{E}$  and the propagator

$$G(\varepsilon) = \sum_j^{\prime} \frac{|\phi_j\rangle\langle\phi_j|}{\varepsilon - E_j}. \quad (6)$$

The sum/integral in (6) runs over the discrete/continuous spectrum of  $\hat{H}_0$ . The series of energies  $\varepsilon_k$  in (5) accounts for successive absorption/emission of photons:

$$\varepsilon_{k+1} = \varepsilon_k \pm \omega \quad \text{for } k > 1 \quad \text{and} \quad \varepsilon_1 = E_i \pm \omega. \quad (7)$$

Obviously, an  $m$ -photon-absorption process can be reached by an infinite number of realizations (7) of absorption and emission of photons. In lowest order perturbation theory (LOPT) only the ‘shortest’ realization, i.e. that with absorption only, is included. How accurate this approximation is can be assessed by examining a special class of realizations (7) which result in no net absorption of photons. This is nothing but the ac-Stark shift of an atomic level due to a monochromatic field given by, e.g. (Delone and Krainov 2000),

$$\delta E_i(\omega) = \frac{\mathcal{E}^2}{4} \sum_j^{\prime} |\langle \phi_i | D | \phi_j \rangle|^2 \frac{2E_{ij}}{E_{ij}^2 - \omega^2} := \frac{\mathcal{E}^2}{4} \chi_i(\omega), \quad (8)$$

with the time-dependent polarizability  $\chi_i(\omega)$  of the eigenstate  $\phi_i$  to  $\hat{H}_0$  and  $E_{ij}$  the energy difference between the states  $i$  and  $j$ . For bound states the shifts are typically  $\delta E_i(\omega) \approx \frac{\mathcal{E}^2}{4} \chi_i(0) \ll E_{ij}$ ; Rydberg or continuum states, however, are shifted by  $\delta E_i(\omega) \approx \frac{\mathcal{E}^2}{4\omega^2} \gg E_{ij}$ , i.e., by the ponderomotive or quiver energy

$$E_{\text{pond}} = \frac{\mathcal{E}^2}{4\omega^2}, \quad (9)$$

which is the cycle-averaged kinetic energy of a free electron in a laser field of electric field strength  $\mathcal{E}$  and frequency  $\omega$ .

The neglect of such higher order terms, which among other things induce the ac-Stark shift, is the most important error in LOPT. To quantify this error and to see when perturbation breaks down, one may define a critical intensity<sup>5</sup>

$$I^* \sim \mathcal{E}^2 \sim 4\omega^2 \Delta E, \quad (10)$$

<sup>5</sup> Such critical intensities may also be defined by comparing rates from LOPT and the next order, which includes  $m+2$  steps in equation (5) for an  $m$ -photon-absorption process (Faisal 1987) or by comparing rates of above-threshold  $(k+1)$ -photon and threshold  $k$ -photon ionization (Delone and Krainov 2000).

**Table 1.** Laser intensities  $I^*$  marking the border between perturbative and non-perturbative ionization according to equation (10) for various laser wavelengths  $\lambda$ /frequencies  $\omega$ . Note that the breakdown of LOPT, often referred to as the breakdown of perturbation theory, occurs for even smaller intensities (Faisal 1987, Delone and Krainov 2000).

$\lambda$ (nm)	780	100	3.5
$\omega$ (eV)	1.59	12.4	350
$I^*$ (W cm <sup>-2</sup> )	$5 \times 10^{14}$	$3 \times 10^{16}$	$2 \times 10^{19}$

with  $\Delta E$  a typical energy difference (e.g. ionization potential) of the atom. The first indication of the breakdown of LOPT was observed in photoelectron spectra of atoms showing above-threshold ionization (Agostini *et al* 1979, Kruit *et al* 1983, Yergeau *et al* 1986).

Note the quadratic dependence of  $I^*$  on the laser frequency  $\omega$ . As a consequence, perturbation theory applies at high frequencies even for intense laser pulses. To illustrate this, we quote in table 1 the critical laser intensities  $I^*$  according to equation (10) for various laser frequencies  $\omega$ , assuming  $\Delta E = 1$  au.

A similar relation as equation (10) can be derived by determining at which intensity tunnelling of electrons, clearly a non-perturbative process, becomes important. In other words, we ask for the intensity at which electrons will tunnel through the barrier created by the combined potential of the ion and the laser field in a time smaller than the laser period. To answer this question, Keldysh introduced the parameter  $\gamma = T_t \omega$ , with  $T_t$  the tunnelling time (Keldysh 1965). This now-called Keldysh parameter can be approximately rewritten as

$$\gamma = \sqrt{\frac{\Delta E}{2E_{\text{pond}}}}, \quad (11)$$

where  $E_{\text{pond}}$  is given by equation (9). The value  $\gamma = 1$  distinguishes the perturbative multi-photon regime ( $\gamma \gg 1$ ) from the non-perturbative tunnelling ionization regime ( $\gamma \lesssim 1$ ). The spatial characterization of the strength of an oscillating laser field is particularly relevant for extended systems such as clusters. It is provided by the quiver amplitude, which is the spatial excursion of electron driven by the field

$$x_{\text{quiv}} = \frac{\mathcal{E}}{\omega^2}. \quad (12)$$

This amplitude has to be compared to the radius of the cluster, which is about 50 Å for a xenon cluster with  $10^4$  atoms.

To facilitate later discussions, we summarize in table 2 the Keldysh parameters as well as absolute values of ponderomotive energies  $E_{\text{pond}}$  and quiver amplitudes  $x_{\text{quiv}}$  for the laser wavelengths and intensities used below.

### 3.3. Quantum-mechanical description using DFT

For atomic systems in strong optical fields, i.e. laser intensities  $I \gtrsim I^*$ , one has to solve the full many-body problem (1). Since the Schrödinger equation can be solved numerically (on a grid) only for few-electron systems (Kulander 1987, Parker *et al* 2003), time-dependent density functional theory (TDDFT) has been employed.

**3.3.1. Time-dependent Kohn–Sham equations.** The Kohn–Sham (KS) approach to TDDFT (Gross *et al* 1996) allows us to map the interacting many-particle system onto a non-interacting reference system which possesses exactly the same (time-dependent) density  $\rho(\mathbf{r}, t)$ . Despite

**Table 2.** Keldysh parameter  $\gamma$ , quiver amplitudes  $x_{\text{quiv}}$  and ponderomotive energies  $E_{\text{pond}}$  for long and short laser wavelengths  $\lambda$  at different intensities  $I$ .

Wavelength		Intensity		
		$I = 10^{14} \text{ W cm}^{-2}$	$I = 10^{16} \text{ W cm}^{-2}$	$I = 10^{18} \text{ W cm}^{-2}$
$\lambda = 780 \text{ nm}$	$\gamma$	1.55	0.15	0.015
	$E_{\text{pond}}$	5.67 eV	567 eV	56.7 keV
	$x_{\text{quiv}}$	8.28 Å	82.8 Å	828 Å
$\lambda = 100 \text{ nm}$	$\gamma$	12.1	1.21	0.121
	$E_{\text{pond}}$	93 meV	9.3 eV	932 eV
	$x_{\text{quiv}}$	0.136 Å	1.36 Å	13.6 Å
$\lambda = 3.5 \text{ nm}$	$\gamma$	345	34.5	3.45
	$E_{\text{pond}}$	0.1 meV	0.01 eV	1.1 eV
	$x_{\text{quiv}}$	0.0002 Å	0.002 Å	0.02 Å

this transformation to an effective single-particle problem, which reduces the numerical effort for the solution tremendously, there have been so far only either model calculations where the electron dynamics is restricted to one dimension (Véniard *et al* 2002, Grigorenko *et al* 2002, Bauer and Macchi 2003) or calculations for alkali metal clusters with only one active electron per atom (Suraud and Reinhard 2000, Calvayrac *et al* 2000, Andrae *et al* 2002).

Whereas the ionic cores are treated as classical particles, the  $n$  electrons are described by their density  $\varrho$ , which is given in terms of the time-dependent KS functions  $\psi_k$  as

$$\varrho(\mathbf{r}, t) = \sum_{k=1}^n |\psi_k(\mathbf{r}, t)|^2, \quad (13)$$

with  $\psi_k(\mathbf{r}, t)$  following from the solution of the  $n$  KS equations

$$i \frac{\partial}{\partial t} \psi_k(\mathbf{r}, t) = \left[ -\frac{1}{2} \frac{\partial^2}{\partial \mathbf{r}^2} + V_{\text{KS}}(\mathbf{r}, t) \right] \psi_k(\mathbf{r}, t). \quad (14)$$

The potential in (14) is given as a sum

$$V_{\text{KS}}(\mathbf{r}, t) = \mathcal{E}(t) \cdot \mathbf{r} + V_{\text{ion}}(\mathbf{r}, \{\mathbf{R}\}) + V_{\text{hart}}[\varrho](\mathbf{r}, t) + V_{\text{xc}}[\varrho](\mathbf{r}, t) \quad (15)$$

of the laser impact in dipole approximation, the attractive potential  $V_{\text{ion}}$  of the ions at positions  $\mathbf{R}$ , the Hartree term  $V_{\text{hart}} = \int d^3 r' \varrho(\mathbf{r}', t) W(\mathbf{r} - \mathbf{r}')$  accounting for the electron–electron interaction and an exchange–correlation term  $V_{\text{xc}}[\varrho]$ . The last term accounts for all effects due to the electron–electron repulsion (beside the ‘classical’ Hartree term) and has to be approximated. Realistic approximations of  $V_{\text{xc}}$  for predictive calculations are a matter of current research, e.g. by Lein and Kümmel (2005). For the model calculations of laser–cluster interaction, however, the choice of  $V_{\text{xc}}$  is largely dominated by practical issues, i.e. computational effort for large clusters and many active electrons.

Obviously, realistic three-dimensional description by KS techniques is out of reach for the time being already for moderately sized clusters (some ten atoms). Moreover, the applicability of TDDFT for dynamics way beyond linear response as it occurs for a many-particle system interacting with a strong laser field is also an open question.

**3.3.2. Hydrodynamical equations of motion.** A computationally more tractable DFT approach than that based on time-dependent KS equations is the time-dependent extension of

Thomas–Fermi (TF) theory (Bloch 1933). In the static TF theory, the total energy is given as an explicit functional of the electronic density  $\varrho(\mathbf{r}, t)$

$$E_{\text{TF}}[\varrho] = \int d^3r \varrho \left[ \varepsilon_{\text{TF}}[\varrho] + V_{\text{ion}}(\mathbf{r}, \{\mathbf{R}\}) + \frac{1}{2} V_{\text{hart}}[\varrho] \right], \quad (16)$$

with the internal kinetic energy

$$\varepsilon_{\text{TF}}[\varrho] = \frac{3}{10} [3\pi^2 \varrho]^{2/3}. \quad (17)$$

It is this compact form of the kinetic energy which simplifies the numerical treatment, since no set of single-particle functions is required for the solution as in equations (13) and (14). The explicit spatial dependence of  $\varrho$  reflects spatial inhomogeneities which are typical for finite systems. For time-dependent systems a velocity field  $\mathbf{v}(\mathbf{r}, t) = \frac{\partial}{\partial \mathbf{r}} \phi(\mathbf{r}, t)$  is introduced and a collective kinetic term is added in (16) to arrive at the Hamiltonian functional

$$H[\varrho, \phi] = \frac{1}{2} \int d^3r \varrho (\nabla \phi)^2 + E_{\text{TF}}[\varrho] + \mathcal{E}(t) \cdot \int d^3r \varrho \mathbf{r}, \quad (18)$$

which also contains the interaction with the laser field  $\mathcal{E}$  in dipole approximation. The equations of motion for the ‘fluid’ of electrons can be obtained (Bloch 1933) by variation of the energy functional (18) with respect to  $\varrho(\mathbf{r}, t)$  and  $\phi(\mathbf{r}, t)$ . Replacing  $\phi(\mathbf{r}, t)$  by the velocity field  $\mathbf{v}(\mathbf{r}, t)$  gives the well-known hydrodynamical equations of an ideal fluid,

$$\partial \varrho / \partial t + \nabla(\varrho \mathbf{v}) = 0, \quad \partial \mathbf{v} / \partial t + (\mathbf{v} \nabla) \mathbf{v} = -\varrho^{-1} \nabla P_{\text{TF}}[\varrho] - \nabla \Phi, \quad (19)$$

with the Thomas–Fermi pressure  $P_{\text{TF}}[\varrho](\mathbf{r}, t) = \frac{2}{3} \varrho(\mathbf{r}, t) \varepsilon(\mathbf{r}, t)$  and the potential  $\Phi(\mathbf{r}, t) = V_{\text{ion}} + V_{\text{hart}} + \mathcal{E}(t) \cdot \mathbf{r}$ . Note that the pressure  $P_{\text{TF}}[\varrho]$  is the basic quantum-mechanical component of the otherwise classical hydrodynamical approach (Rusek *et al* 2001). Beside the correct (3D) TF functional (17), an *ad hoc* version of the internal kinetic part  $\varepsilon_{\text{TF}}[\varrho](\mathbf{r}, t) \propto \varrho(\mathbf{r}, t)$  has been employed in a 1D implementation (Brewczyk *et al* 1998, Brewczyk and Rzążewski 1999).

For model clusters, equation (19) has been solved in the jellium approximation with an analytical parametrization (Fomichev *et al* 2003). A numerical solution of (19) has been realized in 1D on a grid (Brewczyk *et al* 1998, Brewczyk and Rzążewski 1999) and in 3D using test particles (Rusek *et al* 2001, Rusek and Orłowski 2005). Another test-particle approach (Fennel *et al* 2004) starts from a Thomas–Fermi ground state and solves the Vlasov equation for the single-particle phase-space distribution. The potential used in this calculation was the effective, i.e. density-dependent, potential in the local density approximation.

**3.3.3. Dynamics of the ions.** The classical equations of motion for the ions

$$M \ddot{\mathbf{R}} = - \int d^3r \varrho(\mathbf{r}, t) \nabla_{\mathbf{R}} V_{\text{ion}}(\mathbf{r}, \{\mathbf{R}\}) \quad (20)$$

are solved simultaneously with the KS equations (14) or hydrodynamic equations (19), respectively. As a result, one obtains direct information about the ionic dynamics, e.g. kinetic energies, whereas observables of the electronic systems are only given in terms of the density.

### 3.4. Nano-plasma model

One of the first phenomenological attempts to understand the ionization dynamics of clusters was the nano-plasma model (Ditmire *et al* 1996). It assumes (quasi-free) electrons inside the cluster which are considered as ‘small plasma balls’ of a spatially homogeneous but

time-dependent density  $\varrho(t)$  to account for the laser-induced dynamics. The assumption of a homogeneous plasma requires clusters larger than the Debye or screening length  $\lambda_D = \sqrt{kT_{\text{el}}/4\pi e^2\varrho}$ , which sets the minimal length scale for a plasma with electron temperature  $T_{\text{el}}$ . For a plasma with a typical density of a solid ( $10^{23} \text{ W cm}^{-2}$ ) at  $kT_{\text{el}} = 1000 \text{ eV}$ , one gets  $\lambda_D \sim 5 \text{ \AA}$ . Hence, only clusters with  $R \gg 5 \text{ \AA}$  can be described with the nano-plasma model.

The time evolution of the density is calculated self-consistently: the electric field  $\mathcal{E}$  inside the cluster depends via the dielectric function  $\varepsilon(\omega)$  on the density  $\varrho$ , and changes of the density  $\varrho$  are caused by ionization due to  $\mathcal{E}$ . The field inside the cluster, assumed to be a sphere, is given by (Jackson 1998)

$$\mathcal{E} = \frac{3}{|2 + \varepsilon(\omega)|} \mathcal{E}_0, \quad (21)$$

with  $\mathcal{E}_0$  the vacuum electric field and the dielectric constant  $\varepsilon$  usually taken in the Drude form (Ashcroft and Mermin 1976)

$$\varepsilon(\omega) = 1 - \frac{4\pi\varrho}{\omega(\omega + i\nu)}, \quad (22)$$

with  $\nu$  the electron–ion collision frequency (Ditmire *et al* 1996). Other mechanisms, such as collisions with the cluster surface or recombination, may contribute to the broadening. Knowing the electric field (21) in the cluster, one may incorporate the various processes that occur on the time scale of the laser pulse ( $\sim 100 \text{ fs} - 1 \text{ ps}$ ) such as ionization, energy absorption or cluster expansion. The optical inner ionization and electron-impact ionization of bound electrons have been treated by rate equations according to Ammosov *et al* (1986) and Lotz (1967, 1968), respectively. The latter process requires knowledge about the velocity distribution of the colliding electrons, whereby the model implies that by electron–electron collisions a Maxwell distribution is always established. This distribution is superimposed by an oscillatory motion due to the driving laser. Assuming that the sinusoidal oscillation is not disturbed by the ionic background, the collisional rates due to thermal energy and the oscillation energy are comparable, if the temperature is of the order of the ponderomotive energy (Ditmire *et al* 1996). Furthermore, the velocity distribution is used to estimate the rate of outer ionization (‘free streaming’) which reduces the electronic density  $\varrho$  in contrast to the mechanisms discussed before which feed  $\varrho$ .

We are now prepared to discuss the cluster heating mechanisms which are crucial to understand the observed high charge states. The (cycle-averaged) energy  $E$  deposited in a cluster with volume  $V$  is

$$\frac{\partial E}{\partial t} = \frac{V}{8\pi} \omega \Im(\varepsilon) \mathcal{E}^2. \quad (23)$$

Using (21) and (22), this rate can be expressed in terms of  $\varrho$ ,  $\omega$ ,  $\nu$  and  $\mathcal{E}_0$  (Ditmire *et al* 1996)

$$\frac{\partial E}{\partial t} = \frac{9V}{8\pi} \omega \frac{\Im(\varepsilon)}{|2 + \varepsilon|^2} \mathcal{E}_0^2 = \frac{9V}{8\pi} \frac{\nu 4\pi\varrho/(\omega^2 + \nu^2)}{|3 - 4\pi\varrho/\omega(\omega + i\nu)|^2} \mathcal{E}_0^2. \quad (24)$$

Obviously, the rate (23) is particularly large for large electric fields  $\mathcal{E}$  in the cluster. They occur in the Drude model for

$$\varrho \sim 3\varrho_{\text{crit}} = 3\omega^2/4\pi, \quad (25)$$

which is also called the Mie resonance (Kreibig and Vollmer 1998).

The different models (Ditmire *et al* 1996, Milchberg *et al* 2001) based on the ideas discussed above are characterized by the determination of the dielectric constant and the rate equations for the various processes that occur on the time scale of the laser pulse

( $\sim 100$  fs–1 ps). Furthermore, the assumption of a homogeneous density  $\varrho(t)$  over the cluster volume (Ditmire *et al* 1996) can be relaxed (Milchberg *et al* 2001), allowing for a radial dependence of the density  $\varrho(r, t)$  and averaging the electric field over the solid angle  $\mathcal{E}(r) = \langle \mathcal{E}(\mathbf{r}) \cdot \mathcal{E}(\mathbf{r}) \rangle^{1/2}$ . Then, the dominant absorption mechanism is resonant absorption at the cluster *surface* where the density is at the critical value in equation (25). This resonance moves inward and is maintained for a long time (typically for the whole pulse of a few hundred femtoseconds) until the maximum of the density at the inner part of the cluster falls below this value (Milchberg *et al* 2001).

### 3.5. Quasi-classical microscopic description

The previous sections have made clear that first-principle quantitative calculations based on TDDFT for realistic clusters are still not possible. On the other hand, phenomenological approaches with realistic parameters are based on assumptions which should be verified. Moreover, mechanisms of energy absorption and other characteristic processes are difficult to extract from full TDDFT calculations. Hence, a number of groups (Rose-Petruck *et al* 1997, Ditmire 1998, Last and Jortner 1999, 2000, Ishikawa and Blenski 2000, Toma and Muller 2002, Siedschlag and Rost 2002, 2004, Saalman and Rost 2003, Jurek *et al* 2004a, Jungreuthmayer *et al* 2005) have resorted to classical molecular dynamics for electrons and nuclei to achieve a microscopic description of the many-particle dynamics which is computationally feasible.

The geometry of rare-gas clusters is obtained by optimization of Lennard-Jones clusters (Wales and Doye 1997). Larger clusters can be constructed using icosahedral symmetry of the atoms; these idealized structures, also called Mackay icosahedra (Hoare 1979), are relaxed using pairwise Lennard-Jones potentials. The potential parameters for the different elements (neon, argon, krypton, xenon) are known from simulation of rare-gas solids (Cucoli *et al* 1993).

The key idea concerning the treatment of the electrons (Last and Jortner 1999) which has proven to provide physical insight and numerical efficiency is the division of the ionization process into *inner* and *outer* ionization<sup>6</sup>. Here, inner ionization means excitation of bound electrons resulting in so-called quasi-free electrons. These quasi-free electrons are not bound anymore to a particular atom but still to the cluster as a whole, which can provide a sufficiently strong space charge to hold the electrons back. Eventually, quasi-free electrons may be further heated until they are ejected into the continuum, which we call outer ionization.

The dynamics of bound electrons with typical oscillation periods of a few attoseconds is not treated explicitly. Rather, one uses a statistical approach to describe it by means of the occupation number of bound levels which may change after each time step. The probability for a particular transition within a time step is calculated as the product of the corresponding rate  $\Gamma$  and the time step  $\Delta t$ . This probability  $p = \Gamma \cdot \Delta t$  is compared to a random number  $\xi$  distributed uniformly in the interval  $[0, 1]$ . A transition takes place if  $p > \xi$ . The rates  $\Gamma$  may crucially depend on the laser (intensity and frequency) and the current state of ion; see sections 3.5.1–3.5.3. For the case of clusters, the Coulomb field of the neighbouring ions and electrons has to be taken into account for a proper description of the inner ionization process.

An inner ionization event ‘gives birth’ to a quasi-free electron, which is subsequently propagated classically along with the ions and other quasi-free electrons with all mutual Coulomb forces included. This propagation accounts for electron–electron and electron–ion scattering which is important because of the high particle density in the cluster volume.

<sup>6</sup> In a strict sense, this is only possible in rare-gas clusters. However, the delocalized valence electrons of metallic clusters should be of minor importance for the creation of the high charge states observed, since these electrons are emitted early in the pulse.

Furthermore, for infrared and VUV frequencies the laser may additionally heat these quasi-free electrons.

*3.5.1. Inner ionization in low-frequency fields.* For the case of low-frequency laser pulses, the inner ionization occurs from top to bottom, i.e., the most weakly bound electron is ionized with the highest probability. For sufficiently high fields (Bethe rule)

$$\mathcal{E} \geq \frac{E_{\text{ip}}^2}{4(q+1)}, \quad (26)$$

the ionization of an electron with the binding energy  $E_{\text{ip}}$  to an ion of charge  $q$  is due to the barrier suppression (above-the-barrier ionization). For weaker fields, the electron may still leave the ion by tunnelling through the barrier. The tunnelling probability may be obtained (Ishikawa and Blenski 2000) from the ADK formula (Ammosov *et al* 1986). Since the formula is derived for a homogeneous electric field, one should be careful for the case of clusters where additional contributions to the electric field from the other particles (electrons and ions) may be important. Therefore, it has been proposed (Siedschlag and Rost 2002) to calculate directly the tunnel integral

$$s = \int_0^1 d\tau \sqrt{V(\mathbf{r}_\tau) - E_{\text{ip}}}, \quad \mathbf{r}_\tau = \mathbf{R} + \tau \mathbf{X}, \quad (27)$$

with the electric total field at the ionic position  $\mathbf{R}$  pointing in the direction  $\mathbf{X}$ , with  $|\mathbf{X}| = 1$ . The potential  $V$  in (27) is composed of the laser and all the other particles, not just the ion under consideration. The tunnelling rate is finally given by the ratio  $P/T_{\text{K}}$ , with the tunnel probability  $P = \exp(-2s)$  and  $T_{\text{K}}$  the Kepler period of the particle orbiting around the nucleus.

Another possibility of inner ionization is due to inelastic collisions of (sufficiently fast) quasi-free electrons with bound electrons: electron-impact ionization. The cross section for this process is taken (Ishikawa and Blenski 2000) from the Lotz formula (Lotz 1967, 1968). Here, a similar problem as above arises. Because the Lotz formula is derived for an isolated collision without cluster environment, one has to extrapolate the velocity of incoming electrons to its asymptotic value.

In order to properly take the environment into account, one may describe the inner ionization classically (Saalman and Rost 2003). One ‘creates’ an electron at a particular ion if there is no other electron bound to that ion. This approach relies only on the top-to-bottom assumption of inner ionization. Although it neglects tunnelling, it accounts simultaneously for barrier-suppression and electron-impact ionization of ions in a cluster environment.

*3.5.2. Inner ionization in VUV fields.* Atomic ionization by 100 nm lasers is perturbative, cf the Keldysh parameters in table 2. Therefore, inner ionization is accounted for by calculating the atomic photoabsorption rates (Rost 1995) for the respective outermost electron of each cluster atom. While for a single atom the photon frequency used at DESY (Wabnitz *et al* 2002) and in calculations (Siedschlag and Rost 2004), namely 12.7 eV, is only sufficient to singly ionize Xe, the situation changes in a cluster environment, where, due to the occurrence of neighbouring charges, the effective threshold for inner ionization is lowered. The situation is schematically depicted in figure 5.

The effective binding energy with respect to inner ionization is thus calculated as

$$E_{\text{eff}} = E_{\text{barrier}} - E_{\text{bind}}, \quad (28)$$

where  $E_{\text{barrier}}$  is the energy of the closest barrier to the atom or ion out of which the electron is to be ionized and  $E_{\text{bind}}$  is the energy of the bound electron (taken to be the purely atomic

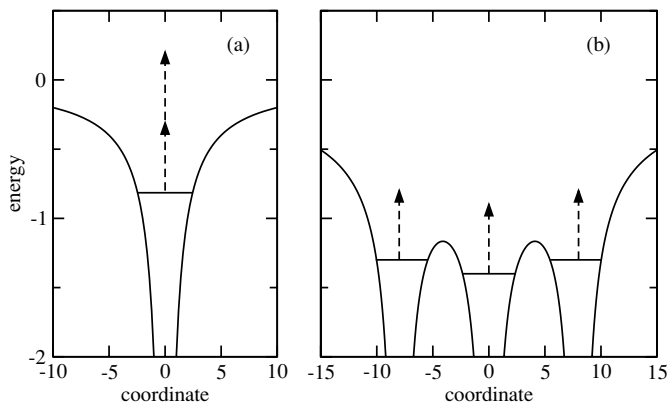


**Figure 5.** Schematic picture of the (inner) ionization process (a) in a single ion (e.g.  $\text{Xe}^+$ ) and (b) in a simple cluster of three ions (from Siedschlag and Rost (2004)). While it takes two photons to ionize the single ion, one photon is sufficient to achieve inner ionization in the case of the cluster.

binding energy plus the additional potential energy due to the laser field and the surrounding charges). Whenever a photon is absorbed and  $\omega > |E_{\text{barrier}}|$ , the outermost electron of the ion is ionized and henceforth treated as a classical particle. This process is, in principle, repeated until all electrons are inner ionized. In practice, however, it turns out that in almost all cases only the 5s and 5p electrons of xenon are ionized.

**3.5.3. Intra-atomic processes in high-frequency fields.** For high-frequency laser impact, ionization proceeds fundamentally different compared to the situation discussed above. Despite the high intensities the laser–atom interaction is of non-relativistic and perturbative nature, cf section 3.2. Ionization starts from the inside because photoionization cross sections  $\sigma$  at x-ray wavelengths are considerably higher for the inner shells than for the valence shells (Amusia 1990). In first-order perturbation theory, cross sections scale as  $\sigma \propto (E_{\text{bind}}/\omega)^{7/2}$  for  $\omega \gg E_{\text{bind}}$ . Typically, the inverse rates are 1–10 fs, i.e., much smaller than the pulse length of about 100 fs. Hence, multiple single-photon ionization is possible, in particular because the inner-shell holes created by photoionization are refilled by Auger-like processes. The Auger decay is only weakly dependent on the atomic charge state<sup>7</sup> and occurs fast, typical times are 0.2–5 fs (Kochur *et al* 1995). Due to this almost instantaneous refilling of the inner shells, they can be ionized many times during the pulse and the atoms can be ‘pumped dry’ efficiently. This occurs ‘inside–out’ and is the exact opposite of the ionization mechanism in the visible wavelength regime where the most weakly bound electrons are removed first. It should be mentioned that this ionization cascade may stop for highly charged ions where the increasing binding energy of the remaining electrons may prevent both photoionization and autoionization, for energetic reasons.

Non-dipole effects in the interaction with single atoms/ions do not have any crucial influence apart from distortions of the angular distribution of the photoelectrons (Cooper 1993). For the interaction with the clusters, they are negligible because of the vanishing impact of high-frequency light on quasi-free electrons as discussed in the following section.

<sup>7</sup> For the idealized case of hydrogenic wavefunctions, it can be shown that the matrix element for Auger decay according to Fermi’s golden rule is completely independent of the nuclear charge.

**3.5.4. Outer ionization.** The classical propagation of the inner-ionized electrons is straightforward apart from two aspects: instability of classical particles and an unfortunate scaling with the particle number. To circumvent the first problem, one may introduce a smoothed Coulomb interaction (Ditmire 1998)

$$W_{ij}(\mathbf{r}_i, \mathbf{r}_j) := \frac{q_i q_j}{\sqrt{r_{ij}^2 + \alpha}} \quad (29)$$

for two particles with charges  $q_i$  and  $q_j$  separated by the distance  $r_{ij}^2 = (\mathbf{r}_i - \mathbf{r}_j)^2$ . Here, the smoothing parameter  $\alpha$  ‘cuts’ the Coulomb potential and prevents the collapse of ions and electrons. The same effect can be obtained by a short-range repulsive part which additionally accounts for elastic scattering (Last and Jortner 1999). Furthermore, for electron–electron pairs, equation (29) simplifies the numerical integration by avoiding strong gradients for close collisions.

Due to the long-range nature of the Coulomb interaction, the calculation of the forces on all  $N$  particles of the systems scales as  $N^2$ . In order to handle clusters with more than  $\sim 10^3$  atoms (including the electrons  $N \sim 10^4$ ), one is forced to use particular algorithms which take advantage of the long-range interactions between a large number  $N$  of particles, e.g., hierarchical tree codes (Pfalzner and Gibbon 1996). Originally developed for gravitational  $N$ -body problems in cosmology (Barnes and Hut 1986), such hierarchical tree codes allow us to follow the dynamics of all charged particles over a few hundred femtoseconds with typical time steps of attoseconds (Saalman and Rost 2003). Alternatively, if the number of atoms is large enough, one can start from the particle-in-cell concept to handle clusters of a few thousand atoms (Jungreuthmayer *et al* 2004). Such clusters with  $N \sim 10^4$  atoms can still be handled successfully with tree codes (Saalman 2006, Saalman and Rost 2005).

In the long-wavelength and the VUV regime, the laser is coupled to the electrons as classical field. The quasi-free electrons are driven over long distances, of the quiver amplitudes in table 2, or experience substantial inverse bremsstrahlung (IBS) heating due to repeated forced collisions with the ions. In the case of high-frequency radiation, the field is oscillating so fast that an electron cannot gain substantial velocity and one can completely neglect the laser field in the classical equations of motion.

Note that despite the short wavelength the dipole approximation would be valid, which becomes apparent by comparing the quiver amplitude with the wavelength, cf table 2. The latter is by orders of magnitude larger, even for high intensities. Furthermore, Compton scattering effects are of minor importance (Jurek *et al* 2004a) due to the low cross section and are also neglected.

## 4. Infrared regime (780 nm)

The vast majority of work on interaction of strong laser pulses with matter has been performed at a wavelength of 780 nm, at which the Ti:sapphire laser operates. This section is structured according to small (up to the order of  $N = 10$  atoms), medium (up to the order of  $N = 10^4$  atoms) and large clusters. However, the number of atoms only indirectly determines different absorption mechanisms. What really matters is the number (density) of quasi-free electrons during the laser pulse as characterized in the introduction, i.e., electrons which are inner ionized but not (yet) outer ionized.

### 4.1. Cooperative behaviour in small clusters

Simulation of the charging in small rare-gas clusters along the lines described in section 3.5 has revealed the existence of an optimum pulse length for maximum charging of the cluster

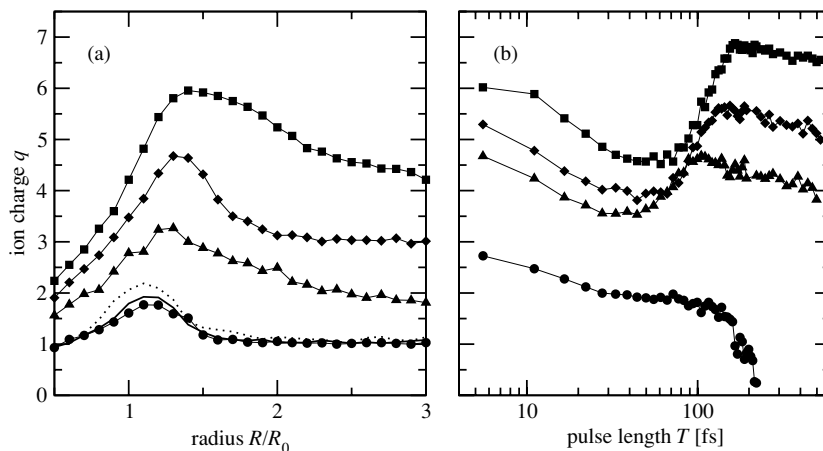


**Figure 6.** Charging of small rare-gas clusters with 16 atoms (a) for fixed atoms in the cluster of radius  $R$  in terms of the equilibrium radius  $R_0$  and (b) as a function of laser pulse lengths  $T$  for different elements: xenon (squares), krypton (diamonds), argon (triangles) and neon (circles). The pulse has the form  $f(t) = F_0 \sin^2(\pi t/T) \sin \omega t$ ,  $0 \leq t \leq T$  with  $T = 55$  fs and  $\omega = 1.5$  eV. The fluency of the laser pulse was kept fixed at the value it assumes for  $F = 0.16$  au (intensity  $8.99 \times 10^{14}$  W cm $^{-2}$ ). The thick solid and dashed lines in (a) are for neon at  $\omega = 2.0$  eV and  $\omega = 3.0$  eV, respectively. Thin lines are to guide the eye.

(figure 6(b)). This optimum pulse length was traced back to an optimum mutual ionic separation  $R_{ei}$ , where ‘ei’ stands for enhanced ionization, in the cluster for maximum absorption which can be seen from holding the ions fixed during the laser pulse and recording the charging of the cluster for different separations  $R$  (figure 6(a)). The mechanism of enhanced ionization was first discovered for diatomic molecules (Seideman *et al* 1995, Zuo and Bandrauk 1995) and applies for small clusters in full analogy. It is characterized by an independence of the laser frequency (as long as its period is adiabatically slow compared to the orbital times of the electrons). For clusters this independence of  $R_{ei}$  from the laser frequency also holds true and is clearly visible for fixed ions (figure 6(a)). However, a slightly different expansion speed of the cluster for different laser frequencies leads to a slight frequency dependence of the experimentally accessible optimum laser pulse length although the mechanism of enhanced ionization is operative. In contrast to diatomic molecules, enhanced ionization occurs in clusters also for circularly polarized light (Siedschlag and Rost 2002). This is easy to understand, since in a (spherical) cluster the rotating polarization vector always finds two ions in a line, which is required for enhanced ionization. As mentioned in section 2.2, there has been so far no experimental proof of enhanced ionization in clusters. The ‘simplest’ way would be to use a laser with a frequency which is higher than the plasmon frequency of the unperturbed cluster. Then, resonant absorption (see the next section) cannot occur and increased ionization could clearly be attributed to the mechanism of enhanced ionization.

Enhanced ionization is in no way a collective behaviour, it is rather the cooperative effect of two ions in line with the instant polarization vector which helps to outer ionize the electron. Clearly, it does not work if there is another shell of ions beyond the outer ion which prevent outer ionization. Hence, enhanced ionization is limited to small clusters. However, the number of atoms of the cluster is not the only limiting factor. Another one is the number of quasi-free electrons generated during the pulse, i.e., those electrons which are inner ionized, but not

immediately outer ionized. These quasi-free electrons may absorb (possibly collectively) energy from the laser pulse, a mechanism which we will discuss next.

#### 4.2. Collective behaviour in medium-sized clusters

The collective behaviour emerges from the possibility to match an internal frequency of the cluster, namely that of the centre-of-mass (CM) motion of the quasi-free electrons  $\Omega$ , with the external driving frequency  $\omega$  of the laser.

In general, considering typical electron densities in the cluster, this frequency is much too high. However, when the cluster expands, the density decreases, and in turn also the eigenfrequency of the quasi-free electrons,

$$\Omega(Q, R) = \sqrt{Q/R^3}. \quad (30)$$

The usual picture, from which this quantitative relation is derived, starts with two spheres of constant but opposite charge density which are shifted with respect to each other along a line out of the force-free equilibrium through the external force (in our case the dipole coupling to the laser field). As a consequence, a restoring harmonic force is generated whose force constant  $\Omega$  provides the eigenfrequency of the collectively excited system of electrons and ions. We will see in the next section that this excitation is identical to a surface plasma excitation<sup>8</sup> of an electron plasma. Since the density is a function of the cluster radius, the frequency is also directly a function of the cluster radius, and the resonance condition

$$\Omega(Q, R_{\text{ra}}) = \omega \quad (31)$$

leads, as in the case of enhanced ionization, to a critical cluster radius  $R_{\text{ra}}$ , where ‘ra’ stands for resonant absorption. However, there are striking differences. Quantitatively, the relation  $R_0 < R_{\text{ei}} < R_{\text{ra}}$  holds, i.e., the radius for enhanced ionization  $R_{\text{ei}}$  is smaller than that for resonance absorption  $R_{\text{ra}}$  but larger than the equilibrium radius  $R_0$ . This has been revealed clearly in (Martchenko *et al* 2005) where both mechanisms, enhanced ionization and resonance absorption, could be identified in a single cluster expansion. Secondly, collective excitation is strongly frequency dependent in contrast to enhanced ionization.

Resonance absorption occurs also in metal clusters for the valence electrons. This requires of course laser fields which must not be so strong that the loosely bound valence electrons are lost immediately by field ionization, typical intensities are up to  $10^{12}$  W cm<sup>-2</sup> (Calvayrac *et al* 2000, Fennel *et al* 2004). Also, as mentioned above, even small clusters exhibit resonance absorption if the number of quasi-free electrons is large enough, see the platinum cluster experiment (Köller *et al* 1999) discussed in section 2.2.

Yet, a typical situation is encountered with a rare-gas cluster of  $10^3$  atoms and more. The energy absorption dynamics is illustrated in figure 7 with the time evolution of characteristic observables. The existence of multiple shells renders the time evolution slightly more complicated. Nevertheless, two clear intervals of increased energy absorption can be identified. The first one, early into the pulse, represents field ionization of atoms. At that time, the cluster has not expanded yet and the electrons bound to the atoms are not influenced by the cluster environment. Later into the pulse—the exact time is determined by the matching condition (31)—the energy absorption rate increases a second time (figure 7(a)). Since the degree of charge per atom grows now from about 1 to more than 6, the mechanism behind this increased absorption must be very efficient. The phase lag between the driving laser field and the CM

<sup>8</sup> The eigenfrequency can be written in terms of the charge density  $\varrho_{\text{ion}}$  (assumed to be homogeneous) as  $\Omega = \sqrt{4\pi\varrho_{\text{ion}}/3}$ . For a neutral system with  $\varrho_{\text{ion}} = \varrho_{\text{quasi}} = \varrho$ , it reads  $\Omega = \sqrt{4\pi\varrho/3} = \omega_{\text{pl}}/\sqrt{3}$  with  $\omega_{\text{pl}}$  the plasma frequency. This is the classical surface plasmon frequency of a spherical cluster (Kreibig and Vollmer 1998).

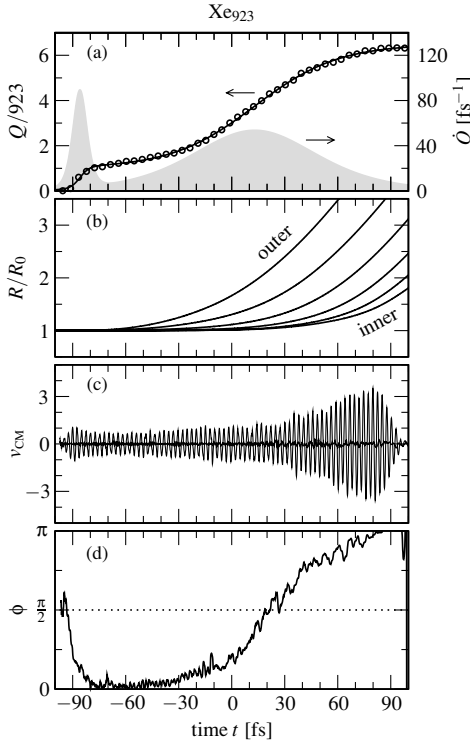


**Figure 7.** Dynamics of  $\text{Xe}_{923}$  in a strong laser pulse ( $\lambda = 780 \text{ nm}$ ,  $I = 9 \times 10^{14} \text{ W cm}^{-2}$ , rise and fall time 20 fs, plateau for  $t = -80$  to  $+80$  fs). All quantities are shown as a function of time  $t$ . (a) Average charge per atom (circles, left axis) and corresponding rate (grey filled line, right axis). (b) Radii  $R$  of all cluster shells in units of their initial radii  $R_0$ . (c) Centre-of-mass velocity  $v_{\text{CM}}$  of the electronic cloud inside the cluster volume. Note that the oscillations are spatially along the linear polarization of the laser, whereas the electron velocity perpendicular to the laser polarization is very small and hardly seen in the figure. (d) Phase shift  $\phi_t$  of the collective oscillation in the laser direction with respect to the driving laser, see text.

electron response passes  $\pi/2$  which proves that resonant absorption is the mechanism in this case (figure 7(c)). Interestingly, the amplitude of the CM electron motion does not increase at resonance which points to a strongly damped dynamics (figure 7(d)). Indeed, the entire CM electron dynamics can be described as the solution  $X(t) = A_t \cos(\omega t - \phi_t)$  to a driven damped oscillator with the equation of motion

$$\ddot{X}(t) + 2\Gamma_t \dot{X}(t) + \Omega_t^2 X(t) = F_0(t) \cos(\omega t). \quad (32)$$

The amplitude  $A_t$ , phase  $\phi_t$ , damping  $\Gamma_t$  and eigenfrequency  $\Omega_t$  are quasi-stationary variables whose change in time, indicated by the index  $t$ , is much slower than the laser period  $2\pi/\omega$ . The four variables are not independent; one can express  $\Gamma_t$  and  $\Omega_t$  in terms of  $A_t$  and  $\phi_t$ ,

$$\Omega_t^2 = \omega^2 + F_0/A_t \cos \phi_t, \quad \Gamma_t = F_0/(2A_t \omega) \sin \phi_t. \quad (33)$$

This allows us to extract the eigenfrequency and damping from the CM velocity, provided it really obeys the dynamics  $X(t)$  of a driven damped harmonic oscillator. The result, along with the determination of the eigenfrequency directly from the density of ions in the expanding cluster, is shown in figure 8. One sees that the damping reaches its maximum with  $\Omega \approx \Gamma$

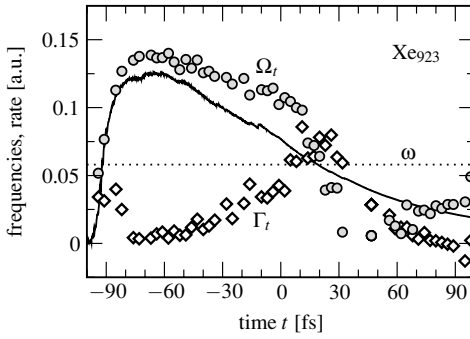


**Figure 8.** Parameters of the harmonic oscillator model (32) as calculated from the  $\text{Xe}_{923}$  dynamics in figure 7. Shown are the eigenfrequency  $\Omega_t$  according to equation (30) as a solid line and from equation (33) with circles, as well as the damping rate  $\Gamma_t$  from equation (33) with diamonds and the laser frequency (dotted line).

at resonance which is in the framework of equation (32) a direct consequence of a roughly constant amplitude  $A$ .

This also holds true for a cluster which contains an order of magnitude more atoms, i.e.  $10^4$  instead of  $10^3$  (Saalmann 2006). The strong change in (negative) slope of the lower energy edge in the electron energy spectrum at  $t \sim 270$  fs in figure 9 is due to a sudden increase of positive background charge which indicates increased outer ionization. The reason is efficient energy absorption since the resonance condition is met as the phase lag of  $\pi/2$  shows (inset of figure 9). However, the laser pulse must be long enough so that the cluster can expand until the resonance condition at low enough electron density is met during the laser pulse.

#### 4.3. Nonlinear behaviour in large clusters

Clusters with  $10^4$ – $10^5$  atoms can be handled numerically with appropriate techniques, such as tree codes (Saalmann 2006, Saalmann and Rost 2005) or specially adapted PIC codes (Jungreuthmayer *et al* 2004). In the latter work, it has been argued that the main heating effect is polarization-induced heating, i.e. a phase difference between the oscillating electron cloud and the driving field which does not originate from resonant absorption<sup>9</sup>. More recently (Deiss *et al* 2005), it was argued that the polarization acts against the dephasing and cannot be responsible for enhanced absorption. In any case, as long as the cloud of quasi-free electrons oscillates over a few laser cycles with the laser frequency, any energy gain from the laser field must be due to a phase difference or non-harmonic motion of the electron cloud with respect to the driving field.

A scenario which realizes such a situation is described by Taguchi *et al* (2004), where the authors simulate a rare-gas cluster right from the start as a plasma of quasi-free electrons of low temperature and eight-fold charged (argon) ions. They find a sharp onset of strong ionization at an ion density which does not allow for collective absorption. Rather, a fraction of the quasi-free electrons have gained sufficient energy to travel through the entire cluster within one laser period. The cluster boundary supplies now the source for the non-harmonic motion in fair analogy to the Brunel heating mechanism (Brunel 1987). As a result, a scaling of the laser intensity necessary for the onset of enhanced energy absorption was derived which agrees

<sup>9</sup> The laser pulse was 100 fs too short to reach the resonance condition.

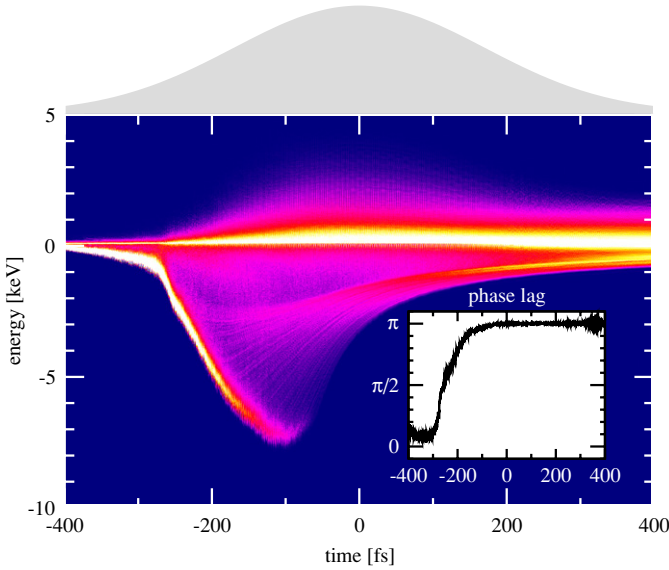


**Figure 9.** Time-resolved energy spectrum of cluster electrons under a laser pulse of the form  $F(t) = \exp(-\log 2(2t/T)^2) \cos \omega t$  with half width (pulse length)  $T = 400$  fs and for a cluster of 9093 xenon atoms. Bright colour corresponds to a large number of electrons. The laser pulse envelope is indicated in grey. The inset shows the phase lag of the electronic CM motion, cf figure 7(d).

well with the simulation results. Whether this cluster ‘edge effect’ can be seen experimentally remains an open question.

One of the few other experimentally accessible, theoretically comparable observables is the distribution of kinetic energies  $E_{\text{kin}}$  of those electrons that have left the cluster. Measurements have shown that these spectra could be fitted by an exponential  $\exp(-E_{\text{kin}}/E_0)$ . In an experiment with clusters of 20 000 xenon atoms illuminated by a 100 fs pulse with  $8 \times 10^{15} \text{ W cm}^{-2}$  peak intensity, the constant was found to be  $E_0 = 700$  eV (Kumarappan *et al* 2003a). The calculation for the same cluster size and laser parameters by Jungreuthmayer *et al* (2004) determined a value of  $E_0 = 800$  eV. This is consistent with the experiment, as are the results from the tree-code calculation (see figure 9) that has a factor 2 fewer atoms. Yet, the spectra obtained for the  $\text{Xe}_{9093}$  cluster (Saalman and Rost 2005) agree well with the experimental result (Kumarappan *et al* 2003a): the calculations yield at the same pulse length an exponential behaviour with  $E_0 = 0.09, 0.33$  and  $1.79$  keV for  $I = 0.8 \times 10^{15}, 4 \times 10^{15}$  and  $20 \times 10^{15} \text{ W cm}^{-2}$ , respectively.

As described in section 3.4, the well-known Mie plasmon resonance, in laser–cluster interaction often simply referred to as the nano-plasma model introduced by Ditmire *et al* (1996), is the linear macroscopic equivalent to the resonance absorption which is therefore expected to supply also an effective absorption mechanism for much larger clusters. However, nonlinear phenomena may modify the picture of the macroscopic nano-plasma model as proposed by Milchberg and co-workers (Milchberg *et al* 2001, Kim *et al* 2003) where the previously assumed homogeneous density of the quasi-free electrons was relaxed in favour of a radially dependent density, cf section 3.4. This leads to a prediction of a variant of the resonance absorption where only a certain shell of electron density at a time with a well-defined distance from the cluster centre gives rise to an eigenfrequency in resonance with the laser frequency. The appealing picture which emerges from this analysis is a resonant ionization of

thin shells of approximate constant electron density which progresses inwards to the cluster centre. One may call the phenomenon another type of ‘edge effect’ which is related to the fact that a cluster is an object of finite size which has a more or less defined boundary. It must be said, however, that an estimate of the quantitative conditions for this mechanism would make it feasible only in extremely large clusters where other effects (such as electron screening and opacity) will play an increasingly important role.

A non-homogeneous electron density was also the starting point of investigations which emphasized that this would lead to components of the electric field the quasi-free electrons form which does not only oscillate with the fundamental laser frequency but also with multiples of it leading to the prediction of resonance enhanced low-order harmonic radiation (Fomichev *et al* 2005). Clearly, such high-order components do not influence the energy absorption of the cluster since they are orthogonal to the laser driving frequency.

Another electron heating mechanism, namely nonlinear resonance absorption based on the oscillation between two rigid spheres of opposite charge (electrons and ions) beyond a linear excursion (Parks *et al* 2001), has been discussed by Mulser *et al* (2005). This effect is predicted to become dominant for very large clusters and at relativistic laser intensities ( $10^{17}$ – $10^{18}$  W cm<sup>-2</sup>). Moreover, the effect has been derived within a model since clearly, numerical simulations are very difficult in the relevant parameter regime.

The approach by Deiss *et al* (2005) as well as that by Santra and Greene (2003) for the VUV situation, discussed in section 5, is an example for an interesting alternative to all other theoretical descriptions. Both groups describe in a detailed way the electron–ion interaction in the cluster and model the rest of the cluster in a more approximate way. Deiss *et al* (2005) advocate a heating mechanism which relies on a large cross section for backscattering of quasi-free electrons from (non-Coulombic) ion potentials. Through this backscattering the back feeding of energy from the electrons into the laser field is converted into a further heating of the electrons. This effect is estimated to lead to a tenfold enhancement in x-ray production (Deiss *et al* 2005) which has a surprising low threshold as recent experiments reveal (Prigent *et al* 2005). Such an ansatz is not, or at least not as seriously as microscopic simulations, limited in the cluster size which can be treated. Moreover, atomic structure can be taken into account more accurately in such an approach, of course, at the expense of possible cooperative or collective effects of all cluster particles which may be influenced in addition by the finite size of the cluster. In particular, the cluster boundary turns out to have a major impact on energy absorption as detailed above. Yet, for high energies, atomic structure becomes increasingly important due to the short wavelengths involved and the atomic modelling may be an interesting alternative to the full simulation of all cluster particles.

## 5. VUV regime (100 nm)

The VUV regime is characterized by photon energies of the order of 10 eV. One such photon is typically sufficient to singly ionize an isolated rare-gas atom; further ionization, however, would require the simultaneous absorption of two or more photons, which, at the intensities available today in this frequency regime, is usually unlikely to happen. For an atom in a cluster environment, the situation is quite different: the influence of the surrounding charges can lead to a notable enhancement of multiphoton processes, thus leading to unexpectedly high absorption rates as observed in the pioneering DESY experiment (Wabnitz *et al* 2002). This regime of laser–cluster interaction has not been studied for a very long time. Yet, there are already several theoretical suggestions to quantitatively explain the increased energy absorption observed.

### 5.1. Quasi-classical models

Given the relative success of quasi-classical models in the IR domain, it seems logical to try a similar approach also for VUV radiation. One objection one might have in this connection is the neglect of resonance effects that might be of importance in the photoionization process. However, the results of the Hamburg experiment (Laarmann *et al* 2004) indicate that details of the atomic structure do not play a significant role once the intensity is higher than approximately  $10^{11} \text{ W cm}^{-2}$ . Hence, it seems entirely appropriate to treat the cluster, just like in the IR case, as a classical ensemble of particles. Of course, the inner ionization process can no longer be described by tunnelling, so that the numerical description has to be modified accordingly.

Apart from Wabnitz *et al* (2002), whose simulations have already been discussed in section 2.3, two groups have followed this road so far: Bauer (2004a, 2004b) and Siedschlag and Rost (2004). In both works, the findings of the Hamburg experiment could be qualitatively reproduced. Due to the inherent quadratic scaling of the execution time of molecular dynamics codes with the particle number  $N$ , relatively small clusters with  $N \leq 80$  were studied, extending to  $N \approx 1000$  with a more sophisticated integration scheme (Jungreuthmayer *et al* 2005).

When describing a multi-electron system in a quasi-classical way, one of the conceptual problems one encounters is to ensure the stability of the (electronic) initial state. Bauer used a momentum-dependent potential in addition to the usual Coulomb potential to describe the interaction of electrons and nuclei, namely

$$V_{\mathbf{r},\mathbf{p},\xi,\alpha,\mu} = \frac{x_i^2}{4\alpha r^2 \mu} \exp \left[ \alpha \left( 1 - \left( \frac{\mathbf{r}\mathbf{p}}{\xi} \right)^4 \right) \right], \quad (34)$$

where  $\mu$  is the reduced mass of the electron,  $\alpha$  controls how strictly the pseudo-Heisenberg uncertainty relation  $rp \geq \xi$  is fulfilled and  $\xi$  is a free parameter which can be tuned to reproduce the quantum-mechanical energy levels as closely as possible. The great advantage of using the potential given in equation (34) lies in the fact that multi-electron atoms relax into a stable ground state, which consists of all electrons at fixed positions in space with zero momentum. Hence, the non-equilibrium time evolution that follows when switching on a laser field can be described in a fully self-consistent way, without any further approximations. It has been shown that calculations employing the potential given in equation (34) can reproduce the relative abundance of ions in intense field laser-atom interactions quantitatively (Bauer 2004a), thus making it reasonable to use it in many-atom systems as well.

In the first paper (Bauer 2004b),  $N_e$  was restricted to 3, which, of course, was not sufficient to reproduce the charge states of 6+ and higher observed at DESY. However, some general trends could be established: firstly, it was shown that a single atom responded more sensitively to VUV (100 nm) than to IR (780 nm) radiation as long as the intensity remained below  $10^{15} \text{ W cm}^{-2}$ . The pulse length was 42 fs in both cases. This result is not implausible considering the huge single photon cross section for Xe (Samson 1966). Furthermore, in the intensity regime used at DESY (i.e.  $I \approx 10^{13} \text{ W cm}^{-2}$ ), the calculations of Bauer indicated that mainly singly charged ions should result from the interaction of a single Xe atom with an FEL pulse in accordance with the experimental results as published by Wabnitz *et al* (2002). Note, however, the apparently strong dependence of the single atom result on the mode structure of the laser, as indicated in the previous section.

Bauer then moved on to investigate  $\text{Xe}_{27}$  both under 780 nm and under 100 nm irradiation. His model resulted in an *average charge* per atom which was lower for the cluster than for the single atom, with the VUV radiation being more efficient than the IR pulse. The *inner ionization* was seen to be very efficient for both frequencies and attributed to *ionization ignition*, meaning that the binding energies are effectively lowered once the charged ions are present

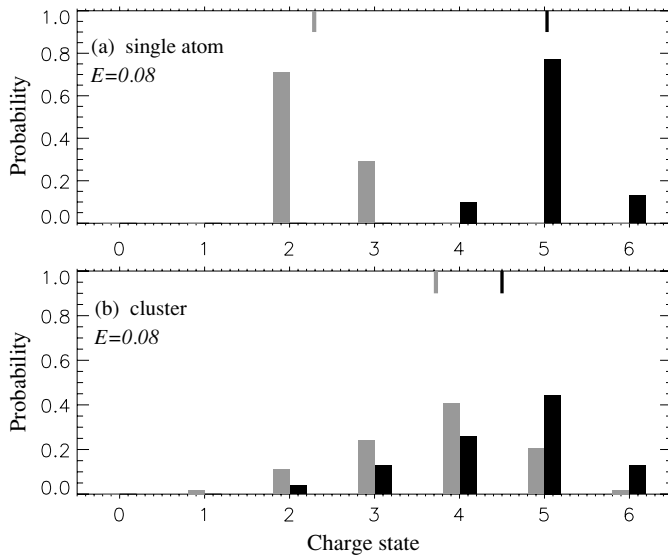


**Figure 10.** Ionic charge states for a single atom and a Xe<sub>54</sub> cluster (from Bauer (2004a)) for 800 nm (grey) and 100 nm (black). The narrow bars at the top of the panel indicate the average charge states.

in the cluster. Hence, the cluster quickly turns into a nano-plasma in which the electrons can gain energy by collisions with the ions (inverse bremsstrahlung). Consequently, also the energy absorption per atom was calculated to be higher for the cluster than for the single atom, although not in the regime of 30 absorbed photons per atom as measured at DESY.

The same qualitative picture (good absorption of VUV radiation due to reduced effective ionization potentials and a high number of IBS processes) could be confirmed in the second paper by Bauer on this topic (Bauer 2004a). The modelling was identical to the previous work; however, with increased computational power, Xe<sub>54</sub> clusters with  $N_e = 6$  active electrons per atom could be studied. With a field strength of  $\mathcal{E} = 0.08$  au in a 42 fs, 100 nm pulse (corresponding to an intensity of  $I = 2.25 \times 10^{14}$  W cm<sup>-2</sup>), an average ionic charge state of  $q \approx 2$  has been predicted. All six electrons per atom were seen to be inner ionized during the pulse; while this might be interpreted as a hint towards the need for increasing the number of active electrons, Bauer followed the evolution of those electrons that, although they are inner ionized, are quickly recaptured by another ion in the cluster. This analysis showed that the effective charge of ions inside the cluster was only about  $q \approx 4$ , so that the number of active electrons included in the calculations seemed not to form an unphysical limit to the inner ionization process.

With  $\mathcal{E} = 0.08$  au, which is about four times higher in intensity than in the Hamburg experiment, ionic charges of up to 6+, with an average of more than 4, were calculated (see figure 10). However, it should be noted that these high charge states partially result from the definition of an atomic ionization process, namely, taking every electron as ionized that is further away from any ion than a Wigner–Seitz radius  $r_{WS}$ . With  $r_{WS} = 4$  au only, it is clear that there are quite a few electrons with negative total energy which, however, do not fall into this category. This also explains the inconsistency of the charge states shown in figure 10 with the average number of electrons which have actually left the cluster, which was seen to be about 2.

Siedschlag and Rost (2004) have developed an alternative model for VUV light–cluster interaction. There are two differences to Bauer’s approach: the inner ionization process is described in a strictly sequential manner using modified single photon ionization rates, and the number of electrons included is not limited *a priori*. It is a modification of the approaches used for low-frequency fields and has been described in section 3.5.2. Calculations showed that inner ionization happens during the first few femtoseconds of the pulse, so that most of the time the cluster is a nano-plasma with up to eight electrons per ion. Taking Xe<sub>80</sub> clusters irradiated by a pulse analogous to that used at DESY, it could be shown by Siedschlag and Rost (2004) that about 80% of the absorbed energy comes from IBS processes (the rest is contributed by the energy of the photons absorbed in the inner ionization process). The decisive difference between the simulations done in Hamburg (Wabnitz *et al* 2002) and partly also those done by Bauer is that the average charge of the ions in the nano-plasma is almost 8+; when one looks at the analytical expression for the energy absorption rate of a plasma by IBS processes given by Krainov (2000),

$$\left\langle \frac{dE}{dt} \right\rangle = \frac{4\pi^{3/2}q^2q_{\text{ion}}I}{15 \times 35^6\omega^2\sqrt{2T}} \left( \frac{2}{q\omega} \right)^{2/3} \frac{\Gamma(1/3)}{\Gamma(2/3)}, \quad (35)$$

where  $q$  is the average ionic charge,  $q_{\text{ion}}$  is the ionic density,  $I$  is the laser intensity and  $T$  is the temperature of the electrons, it becomes clear that the dependence on the ionic charge goes as  $q^{4/3}$ . Hence, an ionic charge of 8 should lead to an increase in energy absorption by a factor 6.35 compared to the charge of  $q = 2$  used in the simulations in Wabnitz *et al* (2002), which nicely explains the gap between the 85 eV energy absorption per atom found in these simulations and the 400 eV per atom measured in the experiment.

Due to the quadratic scaling of the many-body Coulomb interaction used in Siedschlag and Rost (2004) with the number of particles, the calculations in the cited work have been limited to clusters with  $N \leq 80$ . For this cluster size, the final charge distribution is in good agreement with experiment, as can be seen in figure 11. Of course, a meaningful comparison with experiment can only be made after an integration over the focal volume of the laser has been performed. The charge spectrum resulting from the interaction of clusters directly in the laser focus (which is shown in figure 11(a)) extends to higher charge states than the spectrum averaged over the focal volume (figure 11(b), circles; the experimental results are indicated by crosses). Note that, according to these calculations, a remarkably high number of neutral atoms are predicted. These neutral atoms could not be detected with the setup used in the DESY experiment; they originate from the centre of the cluster, as the electrons in the nano-plasma that is created by the VUV pulse are pulled inwards by the approximately spherically symmetric potential of the ions. The high charge states, conversely, originate from the cluster edge. Such a pronounced imbalance of electronic charge would occur under IR laser light only for much larger clusters with a much larger space charge. It is needed to overcome the quiver motion (see table 2) of the electrons, which on the other hand is small under VUV light.

Jungreuthmayer *et al* (2005) have recently performed molecular dynamics calculations using a tree code (Barnes and Hut 1986) which enabled them to treat larger cluster sizes of up to Xe<sub>1000</sub>. In this work, there are two ways that a bound electron can be inner ionized: the outermost electron in each Xe atom can absorb a single photon, which happens with a probability calculated by quantum-mechanical single-photon ionization rates for the ground state of a Xe atom. Further inner ionization can take place by electron-impact ionization, which has been modelled using Lotz cross sections. As in the previously described quasi-classical approaches to VUV light–cluster interaction, the authors of this work have found that the light pulse quickly turns the cluster into a nano-plasma. However, they propose a new heating mechanism, different from inverse bremsstrahlung, which they state to be

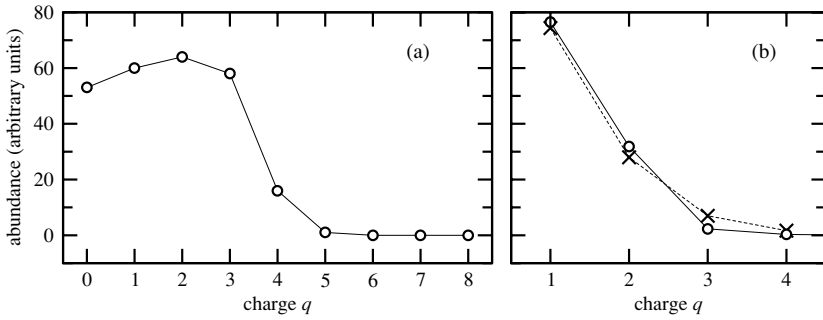


**Figure 11.** Abundance of ionic charge states of Xe<sub>80</sub> after irradiation from a soft x-ray pulse: (a) yield in the focus of the pulse; (b) yield integrated over a Gaussian (spatial) pulse profile (circles: calculations from Siedschlag and Rost (2004); crosses: measurements from Wabnitz *et al* (2002)).

responsible for the majority of the energy absorbed by the electrons in the cluster. Many-particle recombination heating (MRH) can best be described as a sequence of Auger processes followed by photoionization. Due to the high degree of coupling in the nano-plasma, the probability of two or more already inner-ionized electrons being close to an ion is relatively high, which will very often lead to one electron being recaptured by the ion while the other electron gains the capture energy. The captured electron is then again able to absorb a photon and become inner ionized once more. This cycle can repeat many times during the duration of the pulse, leading to an efficient heating of the electron cloud.

For Xe<sub>1000</sub> and a peak intensity of  $7 \times 10^{13} \text{ W cm}^{-2}$ , Brabec and co-workers obtained an average final ionic charge state of about 4, which is higher than experimentally observed. The difference is attributed to the fact that no averaging over the spatial laser distribution has been performed. A simple model (Siedschlag 2002) for the energy stored in a cluster of  $N$  ions with an average charge of  $q$  and a Wigner–Seitz radius  $r_{\text{WS}}$  yields a Coulomb explosion energy of

$$E_{\text{CE}}(N) = \frac{3}{5} \frac{N^{5/3} q^2}{r_{\text{WS}}}. \quad (36)$$

For a Xe<sub>1000</sub> cluster with  $q = 4$  and  $r_{\text{WS}} = 4.2$ , this leads to an average absorption of about 500 photons per atom to account for this energy, at least in the laser focus. Hence, the MRH mechanism leads to noticeably higher energy absorption than predicted by the other quasi-classical calculations.

## 5.2. Thomas–Fermi calculations

A method that has become quite popular in intense-field–many-body interactions is based on the Thomas–Fermi approximation for the electron density (see section 3.3.2). Rusek and Orłowski (2005) have calculated the response of argon clusters to fs pulses in the IR as well as in the VUV regime. They used Gaussian test particles to describe the electronic density, while the nuclei were classical point particles moving under the influence of their mutual Coulomb repulsion as well as of the mean field force from the electronic density.

Their calculations for the VUV case were done using a photon frequency of  $\omega = 12.7 \text{ eV}$  and an intensity of  $10^{14} \text{ W cm}^{-2}$  with an FWHM pulse length of 50 fs. The results showed a strong dependence on the width of the Gaussian function used to describe the test particles: if the width was chosen relatively small, such that in the ground state of the cluster all electrons were well localized in the vicinity of their respective atoms, the cluster hardly

reacted on irradiation and survived the pulse without significant damage. If, on the other hand, the width was increased such that already in the ground state the electrons were well distributed throughout the cluster, an absorption of about 5 photons per atom for Ar<sub>55</sub> and about 20 photons per atom for Ar<sub>147</sub> was observed. Ionization took place primarily in the outer shell of the cluster, in accordance with the observations by Siedschlag and Rost (2004). The electron density inside the cluster was heated sufficiently to lead to a slow, probably hydrodynamic, expansion of the cluster. The final charge states of the ions were seen to be  $q \approx 2$ .

### 5.3. Statistical modelling

A complementary approach to laser–rare-gas cluster interaction in the VUV regime has been taken by Santra and Greene (2003). They treated the cluster as an infinite plasma which is heated by the irradiation with the VUV pulse. In order to explain the enhanced energy absorption, these authors introduced a modified Coulomb potential of the form

$$V_q(r) = -\frac{q + [Z - q] \exp(-\alpha_q r)}{r} \exp(-r/\lambda_D), \quad (37)$$

where  $q$  is the ionic charge,  $Z$  is the nuclear charge and  $\lambda_D$  is the Debye length. The parameter  $\alpha_q$  is introduced in order to lead to a smooth transition from the  $-\frac{q}{r}$  potential for  $\alpha_q r \gg 1$  to  $-\frac{Z}{r}$  for  $r \rightarrow 0$ . This parameter has to be chosen such that the first ionization potential of a single atom is reproduced correctly.

A set of rate equations for the time-dependent probabilities  $n_0(t), n_1(t), \dots$  of the atomic charge states, together with an expression for the time evolution of the electronic temperature assuming inverse bremsstrahlung was the responsible heating mechanism, has been solved using first an ordinary atomic potential and then the modified Coulomb potential of equation (37). It was shown that the use of the latter resulted in an increase in the number of absorbed photons by about an order of magnitude.

The effect of ionization due to electron impact was completely neglected during the pulse. Hence, all atoms in the calculations were only doubly charged at the end of the pulse, clearly not reproducing the experimental results. However, Santra and Greene (2003) argued that heating due to inverse bremsstrahlung and the heating due to (e, 2e) processes were commuting processes. This approximation allowed them to redistribute the resulting amount of energy absorbed by IBS after the end of the pulse assuming a Boltzmann distribution and a common temperature of the electrons and the ions in the cluster. In this way, a prediction for the ionic charge states could be obtained which turned out to be in good agreement with the experimental results. However, one has to keep in mind that this calculation has been performed assuming an infinitely extended cluster, so that any dependence on the cluster size cannot be included in the model. Furthermore, the IBS absorption was calculated using the ionic density of the neutral cluster, and the redistribution of the absorbed energy in order to calculate the final charge states neglected the fact that these charge states are measured well after the disintegration of the cluster, with the ions being far away from each other. Furthermore, cooling effects during the expansion of the cluster and, maybe even more severely, the profile of the laser have been neglected. All that overestimates the charge states or shifts the average charge to higher values.

## 6. X-ray regime (3 nm)

The dynamics of clusters in strong short-wavelength x-ray laser pulses is much less studied and understood than that of clusters exposed to pulses of longer wavelengths. The main reason is

the lack of experimental data. Such data will be available only if the planned XFEL machines (Feldhaus *et al* 2005) at DESY in Hamburg (Materlik and Tschentscher 2001), at the LCLS in Stanford (Arthur 2002) or at BESSY in Berlin (Krämer *et al* 2004) start operating in the next few years.

The first theoretical studies concentrate on the ionization and fragmentation dynamics of various cluster types (Saalmann and Rost 2002, Saalmann 2004, Jurek *et al* 2004a, Bergh *et al* 2004). This is of crucial importance for the planned imaging investigations with XFEL machines. On one hand, the extreme brilliance of the XFEL helps in getting sufficient intensity in the diffraction pattern of a sample in the beam. On the other hand, however, this beam strongly ionizes the sample which will therefore undergo fragmentation. The key question is on which time scale compared to the laser pulse this ‘loss of structure’ occurs. Since atomic clusters will be most likely among the first targets in strong x-ray beams to address this question experimentally, it is appropriate to study the basic ionization mechanism for these systems.

We will mainly discuss the work which treats the dynamics microscopically (Saalmann and Rost 2002, Saalmann 2004, Jurek *et al* 2004a, 2004b). The approaches are similar but differ in the applied laser frequency and the irradiated clusters, i.e. type and size, respectively:  $\hbar\omega = 350$  eV on small argon cluster (Saalmann and Rost 2002) and  $\hbar\omega = 12$  keV on medium-sized carbon clusters (Jurek *et al* 2004a). The first study (Saalmann and Rost 2002, Saalmann 2004) concentrates on the electron dynamics at a frequency which is only slightly larger than the binding energy of the L-shell of argon. This permits insight into the importance of competing excitation/ionization processes. In the other study (Jurek *et al* 2004a, 2004b), the laser frequency was chosen equal to the highest one available in the near future. The main emphasis was put on the question whether x-ray imaging will be possible or not when the atoms are stripped of their electrons and move due to their Coulomb repulsion.

The method for calculating the ionization and fragmentation dynamics has been described in section 3.5. Intra-atomic processes are treated via transition rates, cf section 3.5.3, and free electrons and ions are propagated classically, cf section 3.5.4.

### 6.1. Clusters versus atoms

To start with, we compare the energy absorption and ionization of small clusters with those of atoms (Saalmann and Rost 2002). Figure 12 shows the absorbed energy and the final charge of two different clusters divided by the number of atoms for a photon energy of  $\hbar\omega = 350$  eV. Whereas the charge distribution of the fragments, and thus the average charge, is directly measurable in the experiment, the absorbed energy can only be deduced from the calculation. It is shown here, because it gives direct information on the number of photons absorbed during the pulse, while all the other processes (intra-atomic decay, intra-cluster screening) are not influenced by the laser. As an overall feature, we note a reduced energy absorption and lower final charges for the clusters. At low field strengths,  $\mathcal{E} = 0.1$  au, only about one single photoionization event per atom occurs, independently of the cluster size. The absorbed energy per atom is  $E_{ab} \sim 350$  eV. This energy  $E_{ab}$  increases with the laser field strength to more than 1 keV (i.e. about three to four photoionized electrons per atom) for  $\mathcal{E} = 10$  au. However, values for the clusters are always below those for the atom. This reduction is stronger for the larger cluster. It indicates a considerable influence of the cluster environment on the photoionization process, see discussion in section 6.2. The final charge of the cluster ions, shown in figure 12(b), accounts besides the photoionization also for intra-atomic decays and ‘post-collisional effects’ by propagation of the inner-ionized electrons. Apart from the quite steep rise of the final charge in the atomic case for low fields  $f < 0.3$  au, the overall increase with the field strength  $\mathcal{E}$  is

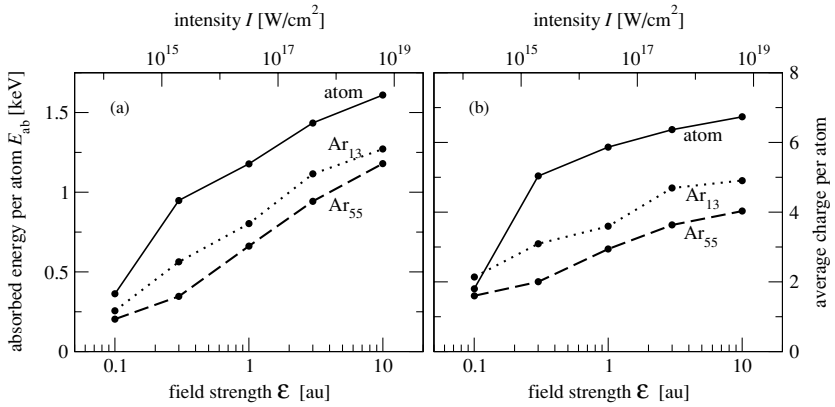


**Figure 12.** Absorbed energy  $E_{ab}$  per atom (a) and final average charge per atom (b) for two cluster sizes  $\text{Ar}_{13}$  and  $\text{Ar}_{55}$  produced by an XFEL pulse ( $\hbar\omega = 350$  eV,  $T = 100$  fs) as a function of the field strength  $\mathcal{E}$  compared to atomic argon as a target. Each point is the average of ten simulations.

weaker in particular for the cluster. Thus, clusters are less effectively ionized at high fields than atoms. As for the energy absorption, the reduction is more pronounced for the larger cluster.

The first reason for the reduced final charge of the cluster is quite obvious: high fields produce a much larger *space charge* in a cluster. Such high space charges suppress ionization, because the absorption of one single photon transfers only a fixed amount of energy to a bound electron. The rapidly oscillating field is unable to drive quasi-free electrons against the positive space charge out of the cluster, which is also evident from the small quiver amplitudes  $x_{\text{quiv}}$  listed in table 2. The space charge effect has also been observed for laser pulses of much higher frequencies. For a 50 fs pulse at 12 keV, the average charge per atom decreases from  $\approx 4.7$  to  $\approx 2.7$ , if the cluster size increases from 50 to 1500 atoms (Jurek *et al* 2004a). Since the electrons held back by the cluster will screen the ionic charges, the explosion dynamics will be altered thereby, as will be discussed in section 6.3.

The explanation for the reduction of the absorbed energy is less obvious. It is due to secondary ionization effects discussed below. Of course, the reduced absorption partly accounts also for a lower final charge of the cluster.

## 6.2. Secondary ionization effects in clusters

As already discussed in section 3.5.3, the inner-shell holes created by photoionization will decay by subsequent ionization processes such as autoionization or shake-off processes. At a first glance, one would expect that such intra-atomic processes are not affected by the cluster environment. However, since the strong laser impact creates local charges in the cluster, at least electrons in weakly bound atomic states are deformed. This is very difficult to quantify for covalent clusters and is therefore usually neglected. In van der Waals clusters with localized electrons, it can be taken into account by including tunnelling, i.e. intra-cluster screening. Practically, one calculates the tunnel probability of bound electrons through the barriers according to equation (27), whereby the barriers are lowered due to neighbouring ions and not by an electric field of a laser. Thus, valence electrons are ‘turned’ into quasi-free electrons which screen local charges. This delocalization of the valence electrons has two consequences: first, the photoionization cross sections become very small since the electrons

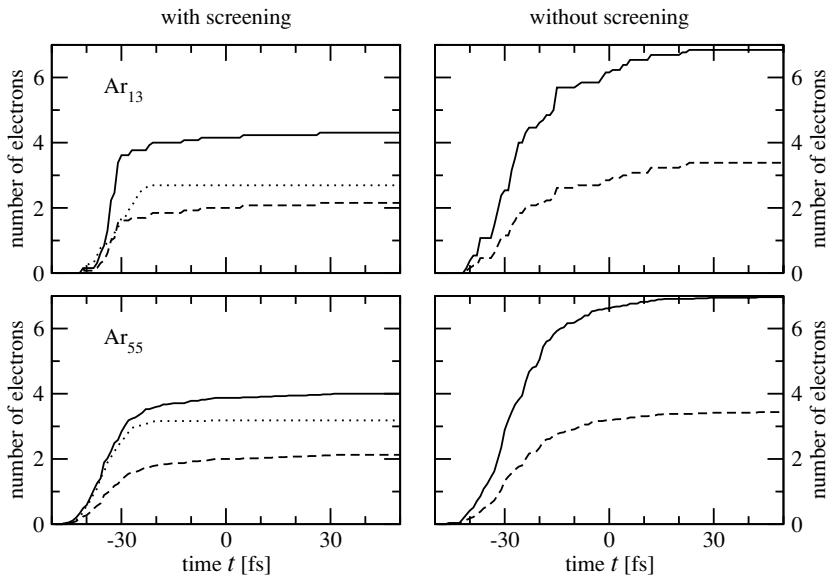


**Figure 13.** Number of created electrons (by photoionization: dashed line; by photoionization and subsequent decays: solid line; by intra-cluster tunnelling: dotted line) as a function of time  $t$  for two cluster sizes Ar<sub>13</sub> (upper row) and Ar<sub>55</sub> (lower row). We compare full calculations (left column) with those where screening, i.e. intra-cluster tunnelling, was excluded (right column). The laser field strength is  $\mathcal{E} = 1$  au, other laser parameters as in figure 12.

themselves are far away from the nucleus. Second, also the Auger decay rates are reduced because the overlap with the core holes becomes smaller.

It is difficult to assign photoionization or autoionization rates to these electrons. However, one can give estimates of these rates using the fact that they depend in a characteristic manner on the energy of the respective bound electron. The quasi-free electrons have a binding energy  $E_{\text{free}}$  (since they are still bound with respect to the full cluster). This energy will be compared to  $E_{\text{bound}}$ , the binding energy of the weakest bound electron in the atom, which is among the bound electrons the most stable one against ionization. Compared to the low rates of the bound electrons, the photoionization rate falls off like  $[E_{\text{free}}/E_{\text{bound}}]^{7/2}$  (Amusia 1990) and the Auger decay rate roughly like  $[E_{\text{free}}/E_{\text{bound}}]^{3/2}$  (Poirier 1988). Due to this scaling, the rates for Ar<sub>55</sub> are reduced during the pulse by factors of about 5 and 20, respectively (Saalman and Rost 2002). Obviously, also those electrons with energies below the barriers are still well above the highest bound electrons and hence fairly delocalized. One has to emphasize that this estimate is an upper bound since the rates decrease even more for higher angular momentum states (Amusia 1990, Poirier 1988) which are likely to be populated by the intra-cluster dynamics. Therefore, we regard it as safe to neglect absorption of photons or autoionization of the quasi-free electrons.

The effect of screening in a cluster can be quantified by artificially excluding tunnelling of electrons to neighbouring ions. Figure 13 shows the result of this (right column) in comparison to a full calculation (left column). Clearly, this artificial constriction of electrons to bound states which corresponds to a localization of the electrons around the ionic cores increases their ionization rates. Note that this applies to primary photoionization and secondary autoionization processes as well. For the full calculation (left column of figure 13), the final number of electrons is reached relatively early in the pulse. To understand this, one may look

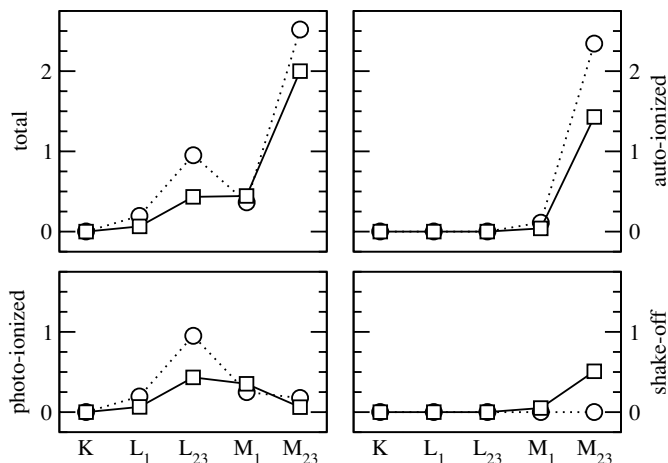


**Figure 14.** Number of electrons per atom for Ar<sub>55</sub> due to photoionization, autoionization, shake-off process and their total sum with respect to the electronic shell they originated from. As in figure 13, full calculations including screening (square symbols) are compared to calculations excluding screening (circles).

at the contributions from particular shells of the atoms. Figure 14 shows the contributing and competing processes resolved for the different shells of argon. The photoionization of the L-shell is suppressed when the binding energy falls below the single-photon threshold. This occurs earlier in the case of clusters due to the valence delocalization which is connected with a reduced electron–electron repulsion within the atom. This faster increase of the L-shell binding energies in clusters explains both the weaker ionization compared to atoms (lower-left part of figure 14) and the earlier saturation in the pulse (left column of figure 13). The latter follows from the fact that excluding tunnelling makes the atoms in the cluster behave like separated atoms (apart from space charge effects). One should emphasize that figure 14 counts only those electrons which are finally free, i.e. have a positive energy, at the end of the pulse. This explains that the dominating sub-shell for photoionization is L<sub>23</sub> with a smaller binding energy than L<sub>1</sub>. In an analogous manner, only electrons from the most weakly bound sub-shell M<sub>23</sub> acquire in a two-electron Auger process enough energy to leave the cluster. Furthermore, figure 14 shows that the delocalization effect is of comparable importance for both photoionization and autoionization.

As we have seen, in addition to simply lower absorption rates the reduction of photon absorption is also due to the fact that the inner shells to be ionized are no longer efficiently refilled by inter-atomic decay, i.e. the atoms in the cluster are temporarily hollow. In order to assess the relative importance of this effect compared to the suppression of ionization due to the cluster space charge, we show in figure 15 the final charges from these restricted calculations for Ar<sub>13</sub> and Ar<sub>55</sub> along with the full calculation for these clusters and the atom. The difference between the two cluster calculations with and without tunnelling (marked by grey shading in figure 15) accounts for the delocalization effect. The difference between the restricted cluster calculation (the dash-dotted line in figure 15) and that for the atom reveals the space charge effect. For field strengths  $f \geq 0.3$  au, where differences between atom and clusters appear, the space charge effect is initially weaker. This changes for stronger fields: whereas for the smaller cluster Ar<sub>13</sub> both are of the same magnitude at  $\mathcal{E} = 10$  au, for the larger cluster Ar<sub>55</sub> the space charge effect dominates at this field strength.

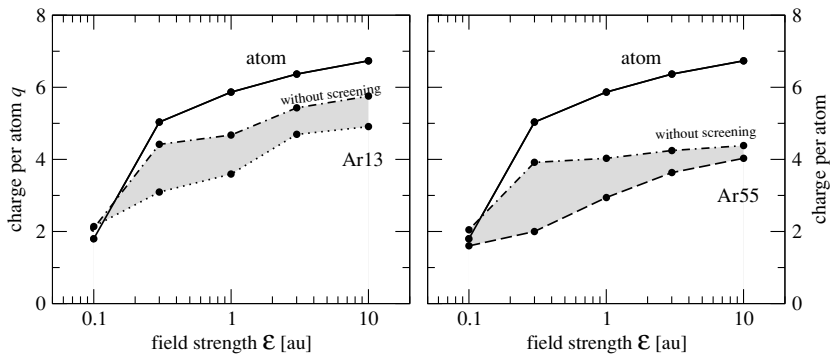


**Figure 15.** Average charge per atom for two cluster sizes Ar<sub>13</sub> and Ar<sub>55</sub> produced by an XFEL pulse (same parameters as in figure 12) as a function of the field strength  $\mathcal{E}$ . Dot-dashed line: restricted cluster calculation where intra-cluster screening was precluded.

Another secondary effect, which has been completely neglected so far, is electron-impact ionization, i.e. inelastic scattering of electrons at atoms. This could be safely done for the systems discussed above for two reasons: first, the mean-free path in such small clusters is much larger than the spatial cluster extension. Second, electrons acquire excess energies dominantly smaller than the energy required to ionize further electrons at the laser frequency considered. This picture changes for larger clusters and higher frequencies. Indeed, it can be seen in figure 16 that the inclusion of electron-impact ionization decreases the observed cluster charge (Jurek *et al* 2004a). It is caused by a redistribution of energy among the electrons. Therefore, fewer electrons possess enough kinetic energy to leave the C<sub>1500</sub> cluster which has high space charge.

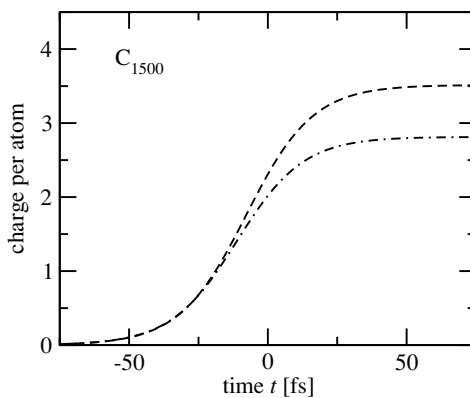


**Figure 16.** Time evolution of charge per atom for a C<sub>1500</sub> cluster in a Gaussian pulse at 12 keV with 50 fs pulse length for two different model calculations with (dashed line) and without (dot-dashed line) electron-impact ionization. After Jurek *et al* (2004a).

### 6.3. Explosion dynamics

In all the cases considered so far, the ionization is typically higher than one electron per atom. This leads to a rapid Coulomb explosion of the cluster. Even for such heavy atoms as xenon it occurs during the XFEL pulse of about 100 fs duration. Of course, the actual explosion

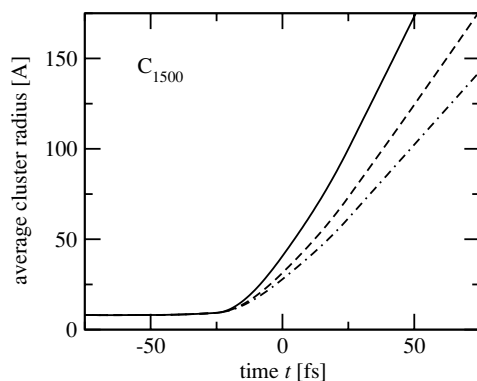


**Figure 17.** Time evolution of average charge of a  $C_{1500}$  cluster in a Gaussian pulse at 12 keV with 50 fs pulse length for three different model calculations neglecting electron screening of ionized electrons (solid line) or taking it into account with (dashed line) and without (dot-dashed line) electron-impact ionization. After Jurek *et al* (2004a).

dynamics depends on the time evolution of the charge of the cluster and is thus a measure of the electronic dynamics. Differences become apparent in particular for larger clusters such as those shown in figure 17. The screening of the quasi-free electrons slows down the expansion considerably, cf. the difference between the solid and dashed curves in figure 17. Taking into account the redistribution of energy by inelastic scattering, i.e. electron-impact ionization (the dot-dashed curve in figure 17), amplifies this effect. Although the atoms/ions have moved already when the laser reaches peak intensity at  $t = 0$ , one may hope to obtain a diffraction pattern from cluster (or molecular) structures which is close to their initial shape. One way to achieve a clear diffraction pattern is to restrict the recording time to the first half of the laser pulse (Jurek *et al* 2004a).

We note that a similar damping of the fragmentation dynamics due to the screening of trapped electrons has been observed for water clusters (Bergh *et al* 2004). Here, free electrons are modelled as a thermalized electron gas. The actual electron distribution is calculated iteratively from the Poisson–Boltzmann equation, the ionic distribution from both the ion–ion repulsion and the electrostatic screening potential of the electrons.

## 7. Summary

The irradiation of clusters with short intense laser pulses leads to many fascinating dynamical phenomena, starting with the different mechanisms how the energy is absorbed from the laser pulse and ending with recombination processes when the charged fragments fly apart. Clearly, there is a confusing number of parameters which influence this behaviour. While some of these parameters are well known and only a matter of choice, others are less well controlled in the experiment, e.g., the size of the cluster or the laser focus. To reach an accuracy and discrimination of models gauged against experiments as for atoms or molecules, reliable convolution procedures or single cluster experiments are needed.

We have concentrated here on laser pulses of some ten to some hundred femtoseconds length and of peak intensity from roughly  $10^{12}$  to  $10^{16}$  W cm $^{-2}$ , i.e., in the non-relativistic domain. Concerning the wavelength of the light, we have mainly discussed 780 nm where most experiments have been carried out, additionally 100 nm light which was available at the free electron laser in Hamburg, and 3 nm light.

Furthermore, we have focused on clusters consisting of some 10 to some  $10^4$  particles, mostly rare-gas atoms. The range in size has been mainly motivated by the possibility of performing microscopic calculations to double check various models and mechanisms for energy absorption and disintegration of the cluster. The main energy absorption mechanism at 780 nm, and so far the only one for which there is considerable experimental evidence, is resonant absorption. It affects almost all optically active electrons in the cluster and dominates therefore any other absorption mechanism. Only if resonant absorption due to a mismatch of parameters is not possible, will subdominant mechanisms become visible. Among those have been proposed enhanced ionization for small clusters, polarization induced dephasing, edge crossing and the so-called Fermi shuttle mechanism. Clearly, clusters can become much larger to form droplets with a size of micrometres instead of nanometres as considered here. While some of the energy absorption mechanisms, e.g., the resonant absorption in its different variants, will prevail for such big species, new phenomena can be expected, particularly opacity effects will begin to become important.

At 100 nm, the situation is completely different and inverse bremsstrahlung is extremely efficient for energy absorption. To date, it is controversial where this efficiency comes from. However, future experiments will certainly clarify the situation.

The upcoming VUV and later XFEL light sources will motivate further cluster experiments which play an important role to study and understand the effect of this radiation on matter. Particularly, the damage threshold is very important to assess with higher accuracy than possible today in rough simulations if and how it is possible to image time-resolved matter on the Ångström scale which is especially interesting for biological matter.

Our knowledge about the intriguing but rather complex dynamics in clusters will also enormously benefit from the upcoming sub-femtosecond or attosecond pulses which will allow us to study the cluster *during* its interaction with a ‘normal’ femtosecond pulse.

## References

- Agostini P, Fabre F, Mainfray G, Petite G and Rahman N K 1979 *Phys. Rev. Lett.* **42** 1127
- Ammosov M V, Delone N B and Krainov V P 1986 *Zh. Eksp. Teor. Fiz.* **91** 2008
- Amusia M Y 1990 *Atomic Photoeffect* (New York: Plenum)
- Andrae K, Reinhard P G and Suraud E 2002 *J. Phys. B: At. Mol. Opt. Phys.* **35** 4203
- Arthur J 2002 *Rev. Sci. Instrum.* **73** 1393 (see also [www-ssrl.slac.stanford.edu/flcls](http://www-ssrl.slac.stanford.edu/flcls))
- Ashcroft N W and Mermin N D 1976 *Solid State Physics* (Philadelphia, PA: Saunders)
- Barnes J E and Hut P 1986 *Nature* **324** 446
- Bauer D 2004a *J. Phys. B: At. Mol. Opt. Phys.* **37** 3085
- Bauer D 2004b *Appl. Phys. B* **78** 801
- Bauer D and Macchi A 2003 *Phys. Rev. A* **68** 033201
- Bergh M, Timneanu N and van der Spoel D 2004 *Phys. Rev. E* **70** 051904
- Bloch F 1933 *Z. Phys.* **81** 363
- Brewczyk M, Clark C W, Lewenstein M and Rzażewski K 1998 *Phys. Rev. Lett.* **80** 1857
- Brewczyk M and Rzażewski K 1999 *Phys. Rev. A* **60** 2285
- Brunel F 1987 *Phys. Rev. Lett.* **59** 52
- Calvayrac F, Reinhard P G, Suraud E and Ullrich C A 2000 *Phys. Rep.* **337** 493
- Chen L M, Park J J, Hong K H, Kim J L, Zhang J and Nam C H 2002 *Phys. Rev. E* **66** 025402
- Cooper J W 1993 *Phys. Rev. A* **47** 1841
- Cuccoli A, Macchi A, Tognetti V and Vaia R 1993 *Phys. Rev. B* **47** 14923
- Deiss C, Rohringer N, Burgdörfer J, Lamour E, Prigent C, Rozet J P and Vernhet D 2005 [www.arxiv.org/physics/0506215](http://www.arxiv.org/physics/0506215)
- Delone N B and Krainov V P 2000 *Multiphoton Processes in Atoms* (Berlin: Springer)
- Dermota T E, Zhong Q and A W Castleman J 2004 *Chem. Rev.* **104** 1861
- Ditmire T 1998 *Phys. Rev. A* **57** R4094
- Ditmire T, Donnelly T, Rubenchik A M, Falcone R W and Perry M D 1996 *Phys. Rev. A* **53** 3379

- Ditmire T, Smith R A, Tisch J W G and Hutchinson M H R 1997 *Phys. Rev. Lett.* **78** 3121
- Ditmire T, Springate E, Tisch J W G, Shao Y L, Mason M B, Hay N, Marangos J P and Hutchinson M H R 1998 *Phys. Rev. A* **57** 369
- Ditmire T, Zweiback J, Yanovsky V P, Cowan T E, Hays G and Wharton K B 1999 *Nature* **398** 489
- Döppner T, Fennel T, Diederich T, Tiggesbäumker J and Meiwes-Broer K H 2005 *Phys. Rev. Lett.* **94** 013401
- Döppner T, Teuber S, Schumacher M, Tiggesbäumker J and Meiwes-Broer K H 2000 *Appl. Phys. B* **71** 357
- Dorchies F, Caillaud T, Blasco F, Bonté C, Jouin H, Micheau S, Pons B and Stevefelt J 2005 *Phys. Rev. E* **71** 066410
- Faisal F H M 1987 *Theory of Multiphoton Processes* (New York: Plenum)
- Feldhaus J, Arthur J and Hastings J B 2005 *J. Phys. B: At. Mol. Opt. Phys.* **38** S799
- Fennel T, Bertsch G F and Meiwes-Broer K-H 2004 *Eur. Phys. J. D* **29** 367
- Fomichev S, Popruzhenko S, Zaretsky D and Becker W 2003 *J. Phys. B: At. Mol. Opt. Phys.* **36** 3817
- Fomichev S V, Zaretsky D F, Bauer D and Becker W 2005 *Phys. Rev. A* **71** 013201
- Fukuda Y, Yamakawa K, Akahane Y, Aoyama M, Inoue N, Ueda H and Kishimoto Y 2003 *Phys. Rev. A* **67** 061201
- Grigorenko I, Bennemann K H and Garcia M E 2002 *Europhys. Lett.* **57** 39
- Grillon G *et al* 2002 *Phys. Rev. Lett.* **89** 065005
- Gross E K U, Dobson J F and Petersilka M 1996 *Topics in Current Chemistry (Density Functional Theory II)* vol 181, ed R F Nalewajski (Berlin: Springer) p 81
- Hagen O F and Obert W 1972 *J. Chem. Phys.* **56** 1793
- Hirokane M, Shimizu S, Hashida M, Okada S, Okihara S, Sato F, Iida T and Sakabe S 2004 *Phys. Rev. A* **69** 063201
- Hoare M R 1979 *Adv. Chem. Phys.* **40** 49
- Ishikawa K and Blenski T 2000 *Phys. Rev. A* **62** 063204
- Jackson J D 1998 *Classical Electrodynamics* (New York: Wiley)
- Jungreuthmayer C, Geissler M, Zanghellini J and Brabec T 2004 *Phys. Rev. Lett.* **92** 133401
- Jungreuthmayer C, Ramunno L, Zanghellini J and Brabec T 2005 *J. Phys. B: At. Mol. Opt. Phys.* **38** 3029
- Junkel-Vives G C *et al* 2002 *Phys. Rev. E* **65** 036410
- Jurek Z, Faigel G and Tegze M 2004a *Eur. Phys. J. D* **29** 217
- Jurek Z, Oszlanyi G and Faigel G 2004b *Europhys. Lett.* **65** 491
- Keldysh L V 1965 *Sov. Phys.—JETP* **20** 1307
- Kim K Y, Alexeev I, Parra E and Milchberg H M 2003 *Phys. Rev. Lett.* **90** 023401
- Kochur A G, Sukhorukov V L, Dudenko A J and Demekhin P V 1995 *J. Phys. B: At. Mol. Opt. Phys.* **28** 387
- Köller L, Schumacher M, Köhn J, Teuber S, Tiggesbäumker J and Meiwes-Broer K H 1999 *Phys. Rev. Lett.* **82** 3786
- Krainov V P 2000 *J. Phys. B: At. Mol. Opt. Phys.* **33** 1585
- Krainov V P and Smirnov M B 2002 *Phys. Rep.* **370** 237
- Krämer D, Jaeschke E and Eberhardt W (ed) 2004 *The Bessy Soft X-Ray Free-Electron-Laser: Technical Design Report* (Berlin: BESSY)
- Kreibitz U and Vollmer M 1998 *Optical Properties of Metal Clusters (Springer Series in Materials Science)* (Heidelberg: Springer)
- Kruit P, Kimman J, Muller H G and van der Wiel M J 1983 *Phys. Rev. A* **28** 248
- Kulander K C 1987 *Phys. Rev. A* **35** 445
- Kulander K C 1988 *Phys. Rev. A* **38** 778
- Kumarappan V, Krishnamurthy M and Mathur D 2001 *Phys. Rev. Lett.* **87** 085005
- Kumarappan V, Krishnamurthy M and Mathur D 2002 *Phys. Rev. A* **66** 033203
- Kumarappan V, Krishnamurthy M and Mathur D 2003a *Phys. Rev. A* **67** 043204
- Kumarappan V, Krishnamurthy M and Mathur D 2003b *Phys. Rev. A* **67** 063207
- Laarmann T, de Castro A R B, Gürtler P, Laasch W, Schulz J, Wabnitz H and Möller T 2004 *Phys. Rev. Lett.* **92** 143401
- Lambropoulos P, Maragakis P and Zhang J 1998 *Phys. Rep.* **305** 203
- Lamour E, Prigent C, Rozet J P and Vernhet D 2005 *Nucl. Instrum. Methods B* **235** 408
- Last I and Jortner J 1999 *Phys. Rev. A* **60** 2215
- Last I and Jortner J 2000 *Phys. Rev. A* **62** 013201
- Lein M and Kümmel S 2005 *Phys. Rev. Lett.* **94** 143003
- Lezius M, Dobosz S, Normand D and Schmidt M 1998 *Phys. Rev. Lett.* **80** 261
- Lotz W 1967 *Z. Phys.* **206** 205
- Lotz W 1968 *Z. Phys.* **216** 241
- Madison K W, Patel P K, Allen M, Price D, Fitzpatrick R and Ditmire T 2004 *Phys. Rev. A* **70** 053201
- Martchenko T, Siedschlag Ch, Zamith S, Muller H G and Vrakking M J J 2005 *Phys. Rev. A* **72** 053202
- Materlik G and Tschentscher T (ed) 2001 *TESLA Technical Design Report, vol V: The X-Ray Free Electron Laser* (Hamburg: DESY) (see also xfel.desy.de)
- McPherson A, Thompson B D, Borisov A B, Boyer K and Rhodes C K 1994 *Nature* **370** 631

- Micheau S, Gutierrez F A, Pons B and Jouin H 2005 *J. Phys. B: At. Mol. Opt. Phys.* **38** 3405
- Milchberg H M, McNaught S J and Parra E 2001 *Phys. Rev. E* **64** 056402
- Mittleman M H 1993 *Theory of Laser-Atom Interactions* (New York: Plenum)
- Mocek T, Kim C M, Shin H J, Lee D G, Cha Y H, Hong K H and Nam C H 2000 *Phys. Rev. E* **62** 4461
- Mulser P and Kanopathipillai M 2005 *Phys. Rev. A* **71** 063201
- Mulser P, Kanopathipillai M and Hoffmann D H H 2005 *Phys. Rev. Lett.* **95** 103401
- Parker J S, Doherty B J S, Meharg K J and Taylor K T 2003 *J. Phys. B: At. Mol. Opt. Phys.* **36** L393
- Parks P B, Cowan T E, Stephens R B and Campbell E M 2001 *Phys. Rev. A* **63** 063203
- Parra E, Alexeev I, Fan J, Kim K Y, McNaught S J and Milchberg H M 2000 *Phys. Rev. E* **62** R5931
- Pfalzner S and Gibbon P 1996 *Many-Body Tree Methods in Physics* (Cambridge: Cambridge University Press)
- Poirier M 1988 *Phys. Rev. A* **38** 3484
- Prigent C, Adouic L, Lamour E, Rozet J P, Vernhet D, Gobert O, Meynadier P, Normand D and Perdrix M 2005 [www.arxiv.org/physics/0506215](http://www.arxiv.org/physics/0506215)
- Rose-Petruck C, Schafer K J, Wilson K R and Barty C P J 1997 *Phys. Rev. A* **55** 1182
- Rost J M 1995 *J. Phys. B: At. Mol. Opt. Phys.* **28** L601
- Rühl E 2003 *Int. J. Mass Spectrom.* **229** 117
- Rusek M, Lagadec H and Blenski T 2001 *Phys. Rev. A* **63** 013203
- Rusek M and Orlowski A 2005 *Phys. Rev. A* **71** 043202
- Saalmann U 2004 *Electron and Photon Impact Ionization and Related Topics 2004 (Institute of Physics Conference Series vol 183)* ed B Piraux (Bristol: Institute of Physics Publishing) p 165
- Saalmann U 2006 *J. Mod. Opt.* **53** 173
- Saalmann U and Rost J M 2002 *Phys. Rev. Lett.* **89** 143401
- Saalmann U and Rost J M 2003 *Phys. Rev. Lett.* **91** 223401
- Saalmann U and Rost J M 2005 *Eur. Phys. J. D* **36** 159
- Samson J A R 1966 *Advances in Atomic and Molecular Physics* vol 2, ed D R Bates and I Estermann (New York: Academic)
- Santra R and Greene C H 2003 *Phys. Rev. Lett.* **91** 233401
- Schroeder W A, Omenetto F G, Borisov A B, Longworth J W, McPherson A, Jordan C, Boyer K, Kondo K and Rhodes C K 1998 *J. Phys. B: At. Mol. Opt. Phys.* **31** 5031
- Seideman T, Ivanov M Y and Corkum P B 1995 *Phys. Rev. Lett.* **75** 2819
- Shao Y L, Ditmire T, Tisch J W G, Springate E, Marangos J P and Hutchinson M H R 1996 *Phys. Rev. Lett.* **77** 3343
- Siedschlag Ch 2002 *PhD Thesis* TU Dresden
- Siedschlag Ch and Rost J M 2002 *Phys. Rev. Lett.* **89** 173401
- Siedschlag Ch and Rost J M 2004 *Phys. Rev. Lett.* **93** 043402
- Smirnov M B and Krainov V P 2004 *Phys. Rev. A* **69** 043201
- Snyder E M, Card D A, Folmer D E and Castleman J A W 1996 *Phys. Rev. Lett.* **77** 3347
- Springate E, Aseyev S A, Zamith S and Vrakking M J J 2003 *Phys. Rev. A* **68** 053201
- Springate E, Hay N, Tisch J W G, Mason M B, Ditmire T, Marangos J P and Hutchinson M H R 2000 *Phys. Rev. A* **61** 044101
- Suraud E and Reinhard P G 2000 *Phys. Rev. Lett.* **85** 2296
- Taguchi T, Antonsen J T M and Milchberg H M 2004 *Phys. Rev. Lett.* **92** 205003
- Ter-Avetisyan S, Schnürer M, Stiel H, Vogt U, Radloff W, Karpov W, Sandner W and Nickles P V 2001 *Phys. Rev. E* **64** 036404
- Toma E S and Muller H G 2002 *Phys. Rev. A* **66** 013204
- Treusch R and Feldhaus J 2003 *Eur. Phys. J. D* **26** 119
- Véniard V, Taieb R and Maquet A 2002 *Phys. Rev. A* **65** 013202
- Wabnitz H 2004 Private communication
- Wabnitz H, de Castro A R B, Gürtler P, Laarmann T, Laasch W, Schulz J and Möller T 2005 *Phys. Rev. Lett.* **94** 023001
- Wabnitz H *et al* 2002 *Nature* **420** 482
- Wales D J and Doye J P K 1997 *J. Phys. Chem. A* **101** 5111 (see also The Cambridge Cluster Database at [brian.ch.cam.ac.uk/CCD.html](http://brian.ch.cam.ac.uk/CCD.html))
- Yergeau F, Petite G and Agostini P 1986 *J. Phys. B: At. Mol. Phys.* **19** L663
- Zamith S, Martchenko T, Ni Y, Aseyev S A, Muller H G and Vrakking M J J 2004 *Phys. Rev. A* **70** 011201
- Zuo T and Bandrauk A D 1995 *Phys. Rev. A* **52** R2511
- Zweiback J, Ditmire T and Perry M D 1999 *Phys. Rev. A* **59** R3166
- Zweiback J, Smith R A, Cowan T E, Hays G, Wharton K B, Yanovsky V P and Ditmire T 2000 *Phys. Rev. Lett.* **84** 2634